ORGANOMETALLICS

pubs.acs.org/Organometallics

Article

Oxalamide-Bridged Ferrocenes: Conformational and Gelation Properties and *In Vitro* Antitumor Activity

Veronika Kovač, Ivan Kodrin, Kristina Radošević, Krešimir Molčanov, Bimalendu Adhikari, Heinz-Bernhard Kraatz,* and Lidija Barišić*

Cite This: *Organometallics* 2022, 41, 920−936

Read Online

ACCESS | Metrics & More | Article Recommendations | Supporting Information

ABSTRACT: The N-termini of the constitutional isomeric ferrocene peptides Boc−NH−Fn−CO−Ala−OMe (**1**) and Boc−Ala−NH−Fn−COOMe (**2**) were deprotected in the acidic milieu and subjected to oxalyl chloride-mediated dimerization to afford the oxalamides −(CO−NH−Fn−CO−Ala−OMe)$_2$ (**3**) and −(CO−Ala−NH−Fn−COOMe)$_2$ (**4**), respectively. The goal compounds were evaluated for their conformational properties, toluene gelation ability, and effect on cell viability of tumor (HeLa, MCF7, HepG2) and normal (HEK293T) cell lines. Detailed spectroscopic analysis in solution revealed the different conformational behavior of constitutional isomers **3** and **4**, and oxalamide **3** was found to have a higher degree of chiral organization due to its involvement in stronger intramolecular hydrogen bonds. Crystallographic analysis showed the presence of two symmetry-independent conformers of compound **3** stabilized by stronger intramolecular hydrogen bonds. The tested compounds self-assemble in toluene to provide supramolecular nanostructures but were unable to form a stable gel. Interestingly, the formation of a stable gel was observed when the toluene solution of **4** was sonicated. Cytotoxic evaluation of **3** and **4** revealed a weaker growth-inhibitory effect on tumor cell lines compared to cisplatin. Oxalamide **3** appeared to be more cytotoxic to HeLa and MCF7 cancer cell lines than to normal HEK293T cells, indicating its potential for drug development as an anticancer agent.

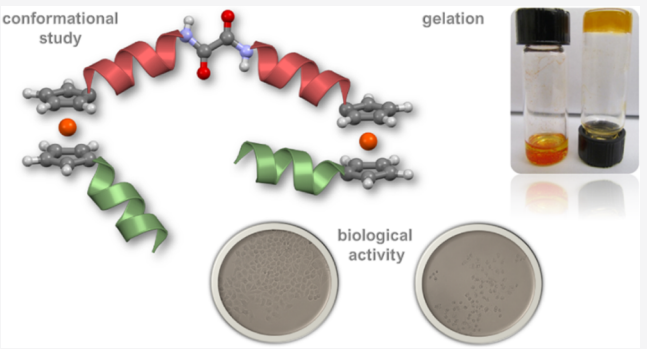

INTRODUCTION

Molecular self-assembly processes are ubiquitous in nature and involve not only macromolecules or their mimics but also small molecules that spontaneously assemble into ordered structures *via* hydrogen bonding, π interactions, hydrophobic interactions, and charge interactions. The self-assembly of small molecules in water or in organic solvents could lead to the formation of a gel consisting of a large amount of a solvent entrapped in a three-dimensional (3D) network of nanosized gelator aggregates.[1−4] Since the aggregates are stabilized by weak noncovalent interactions, various internal or external stimuli (light, sound, pH, solvent, temperature, ions, enzymes) can be used to tune the molecular assembly behavior required for functional expression.[2−7] It is very difficult to predict the gelling ability of a potential gelator as it is closely related to the 3D intermolecular nature of the gel. Therefore, the design and development of simple and effective gelators that exhibit a sharp and rapidly reversible response to one or more stimuli are rather challenging tasks.[8−11] Numerous studies on ferrocene-containing peptides have revealed not only the interesting structural properties resulting from the ability of ferrocene scaffolds to undergo turn nucleation[12−19] but also a potential bioanalytical application.[20,21] Recent work on two ferrocene-modified peptides Phe−Phe (FF) and Phe−Tyr (FY) demonstrated that Fc−FF and Fc−FY (Fc = ferrocenoyl) effectively inhibit insulin fibrillation and thus represent an available strategy for the treatment of amyloid aggregation disease.[22]

Research on ferrocene-containing gelators began with the study of the role of ferrocene in aromatic-mediated intermolecular π interactions in an organogelator consisting of a ferrocene unit linked to a cholesterol group *via* a short peptide linkage.[23] Then, work on Fc−CO−Phe−OH[5] and Fc−CO−Val−Phe−Phe−OMe[4] reported their ability to form hydrogels and organogels, respectively. Our paper on ferrocene peptides containing the short hydrophobic amyloid peptide sequence Aβ(19−21)-FFA highlights the important role of ferrocene as a reliable organometallic scaffold for organogel construction and tuning by controlling the conformation of the

Received: November 29, 2021
Published: April 4, 2022

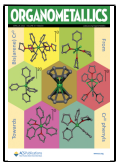

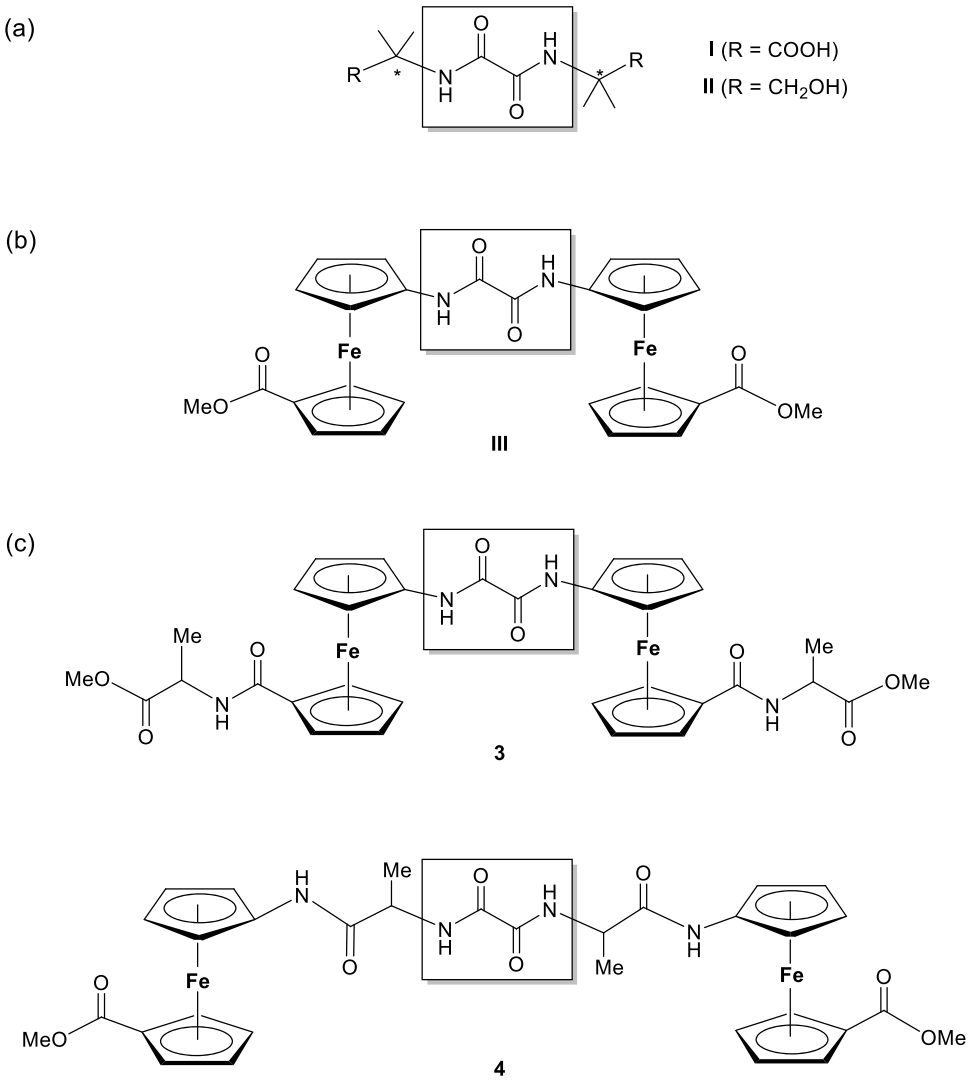

Figure 1. (a) Bis(amino acid) (**I**) and bis(amino alcohol) oxalamide gelators (**II**),[3] (b) ferrocene oxalamide (**III**),[39] and (c) novel ferrocene oxalamides **3** and **4**.

ferrocene core and the proper conjugation of the peptide segments. In addition, intermolecular hydrogen bonding (IHB) has been shown to enhance gelling ability, whereas intramolecular hydrogen bonding impedes gel formation.[24] In addition, we recently provided an overview of stimuli-responsive supramolecular Fc−peptide gels and their corresponding properties with an emphasis on the role of intra- and intermolecular hydrogen bonding in controlling self-assembly.[25]

The ability of structurally diverse organic molecules (amide,[26] urea,[27] cholesterol,[14,28] carbohydrate,[29] aromatic,[30] and organometallic[31] derivatives) to form gels is well described; however, the potential of oxalamides as gel-forming agents is comparatively rarely reported.[3] Their high in-plane hydrogen bonding potential makes oxalamides ideal building blocks in the preparation of self-assembled architectures. Their self-assembly often leads to robust one-dimensional hydrogen-bonded chains, but the insertion of additional hydrogen-bond-accepting or -donating groups allows the formation of more complex structures.

The systematic work of Žinić et al. on the gelation properties of bis(amino acid) (**I**) and bis(amino alcohol) oxalamide (**II**) gelators (Figure 1a) showed that gelation is governed by strong and directional intermolecular hydrogen bonding of the oxalamide units. Moreover, the symmetrical oxalamides that contained achiral amino acids or were meso diastereomers crystallized in contrast to those containing chiral amino acids or amino alcohols, which tended to form gels in certain solvents.[3,32−35]

Recently, bis(amino alcohol)oxalamide was found to efficiently govern the gelation of ionic liquids. Here, the gelation process depended on the size and flexibility of the amino alcohol substituents on the oxalamide moiety.[36] By incorporating the β-sheet peptidomimetic Hao, consisting of hydrazine, 5-amino-2-methoxybenzoic acid, and an oxalamide group, into peptides, Nowick et al. were able to control dimerization against aggregation. While the unnatural amino acid Hao promotes dimerization through β-sheet interactions, the aromatic moiety of Hao prevents multiple strand β-sheet formation.[37] Such antagonization of peptide aggregation is of particular interest for the treatment of protein aggregation diseases, which notably include Alzheimer's disease, Huntington's disease, Parkinson's disease, type II diabetes, and prion diseases.[38]

With these studies in mind, we had synthesized compound **III** containing two ferrocene units connected by an oxalamide

https://doi.org/10.1021/acs.organomet.1c00661
Organometallics 2022, 41, 920−936

Scheme 1. Synthesis of Oxalamides 3 and 4[a]

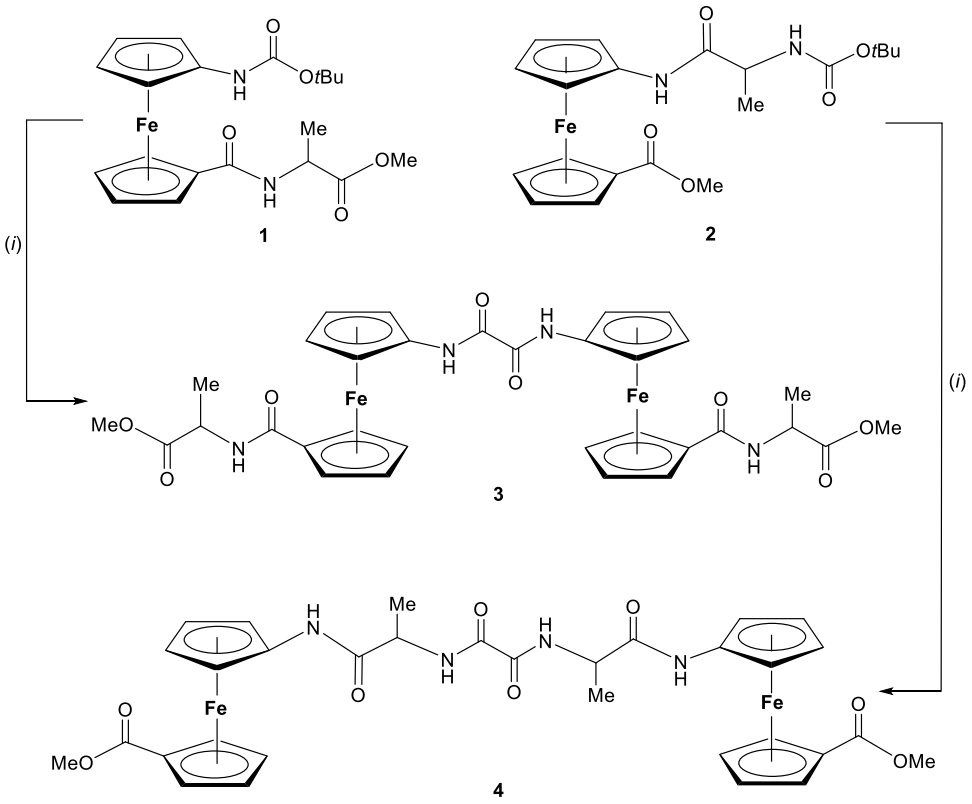

[a](i) 1. $HCl_{gaseous}/CH_2Cl_2$, 2. Et_3N, and 3. oxalyl chloride, pyridine.

bridge (Figure 1b).[39] Spectroscopic analysis in nonpolar CH_2Cl_2 or $CDCl_3$ suggested the conformational pattern based on NH···OC_{COOMe} intramolecular hydrogen bonds (IHBs). In the crystal packing of oxalamide **III**, the adjacent molecules were connected by one N−H···O hydrogen bond and two weaker C−H···O hydrogen bonds, resulting in a staircase-like pattern. The expected motif based on two N−H···O hydrogen bonds between the oxalamide groups of the adjacent molecules was not observed. Although most of the general requirements necessary for the formation of a good gelator [an adequate solubility, the presence of both hydrophilic (oxalamide) and hydrophobic (ferrocene) moieties, and chiral nature][40] were fulfilled, compound **III** tended to crystallize and failed to immobilize the tested solvents. As far as we know, compound **III** is the only example of a ferrocene−oxalamide dimer reported so far.

In this work, we modified the structure of the first reported ferrocene oxalamide **III**[39] by inserting alanine moieties as additional hydrogen bond formation sites to improve the hydrogen bonding and aggregation ability of the resulting ferrocene oxalamides **3** and **4** (Figure 1c). To assess the influence of constitutional isomerism on the hydrogen-bonding behavior and self-assembly of the new compounds, the conformational and gelation properties were investigated.

In addition to gelation, the previously reported oxalamides have been used as pseudopeptide templates in bioorganic and medicinal chemistry,[41] as artificial receptors for biological recognition processes,[42,43] in engineering and crystal design,[44,45] and in coordination chemistry as ligands.[46,47] The *N,N′*-bis(substituted) oxalamides showed anticancer activities.[48−50] The oxalamides have also been evaluated as inhibitors against Alzheimer's disease,[51,52] malaria,[53] and HIV-1.[54] *In vitro* screening of the ferrocene-containing oxalamide **III** showed biphasic dose response characterized by simulation at a low dose and inhibition at a high dose, known as the hormetic effect.[39] Therefore, the potential of the novel ferrocene−oxalamide for both proliferative and cytotoxic activity was also investigated in this work.

RESULTS AND DISCUSSION

Synthesis of Oxalamides 3 and 4. The starting ferrocene peptides **1**[13,14] and **2**[15] were Boc-deprotected in acidic milieu and the hydrochloride salts obtained were suspended in CH_2Cl_2 and Et_3N was added dropwise to pH ∼ 8 to liberate the N-terminus. To prevent rapid decomposition, dichloromethane solutions of the obtained free amines were washed with cold brine to remove Et_3N and then evaporated to dryness. Then, the amines were dissolved in 8 mL of cold CH_2Cl_2 and slowly dropped to the cold mixture of oxalyl chloride and pyridine in CH_2Cl_2. After stirring in an ice bath for 15 min, the reaction mixture was warmed to room temperature and the progress of the reaction was monitored by thin-layer chromatography (TLC). After 2 h, the work-up in the usual manner gave the goal compounds **3** and **4** (Scheme 1). The characterization data with NMR, MS, and IR spectra of compounds **3** and **4** are given in Figures S1−S22, Supporting Information.

IR and NMR Studies. IR spectroscopy has been widely used to analyze hydrogen bonding due to the sensitivity of the C═O and N−H stretching frequencies of the amides to the hydrogen-bonding behavior. In general, a large red shift of the ν(CO) (amide I, 1600−1800 cm^{-1}) and ν(NH) (amide A,

https://doi.org/10.1021/acs.organomet.1c00661
Organometallics 2022, 41, 920−936

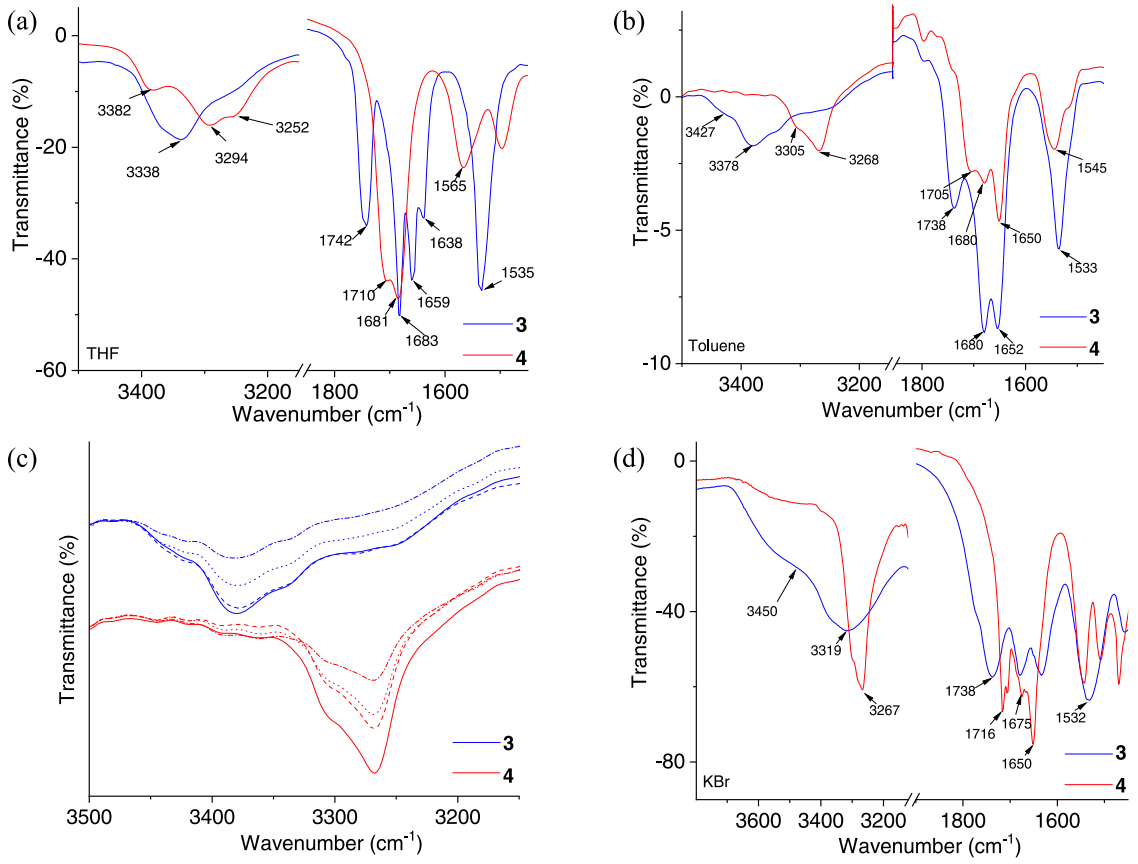

Figure 2. IR spectra of compounds **3** and **4** in (a) THF ($c = 2 \times 10^{-2}$ M), (b) toluene ($c = 2 \times 10^{-2}$ M), (c) NH stretching vibrations in concentration-dependent IR spectra of compounds **3** and **4** in toluene [(—) $c = 2 \times 10^{-2}$ M, (– –) $c = 1 \times 10^{-2}$ M, (---) $c = 5 \times 10^{-3}$ M, (– · –) $c = 2.25 \times 10^{-3}$ M], and (d) IR spectra of compounds **3** and **4** in KBr.

3300−3500 cm^{-1}) frequencies was observed upon their participation in hydrogen bonding.[55−57]

Since the solubility of oxalamides **3** and **4** toward the nonhydrogen bonding solvents $CHCl_3$ and CH_2Cl_2 was too low for IR spectroscopic analysis, a weakly hydrogen-bond-accepting THF was used. In addition, IR spectra were measured in nonhydrogen-bonding toluene since the gelling potential toward toluene was investigated in this work (Figure 2, the concentration of 2×10^{-2} M used was the same for IR and gelation tests). THF was shown to cause the red shift of NH bands when compared to the corresponding peaks in CH_2Cl_2 due to its proton-accepting ability, while a weaker indirect effect on CO stretching was observed.[56,57] Therefore, the red-shifted NH bands in IR spectra of compounds **3** and **4** in THF (Figure 2a) cannot be attributed exclusively to their involvement in hydrogen bonds but also to the possible solvation effect of THF. However, the different hydrogen-bonding properties were indicated by different patterns of the CO regions. The higher absorption bands of the ester CO groups of oxalamide **3** registered at 1742 cm^{-1} indicate that they are not involved in hydrogen bonding, in contrast to the red-shifted ester CO frequencies of its constitutional isomer **4** (1710 cm^{-1}), which are thought to be involved in hydrogen bonding (Figure 2a).[58] Since the CO stretching of oxalamide observed at ∼1682 cm^{-1} has been shown to belong to its free state,[59] the oxalamide CO groups of compounds **3** (1683 cm^{-1}) and **4** (1681 cm^{-1}) are not believed to be involved in hydrogen bonding. Compared to oxalamide **4**, the red-shifted amide CO groups of **3** (1659 cm^{-1}) are more likely to participate in hydrogen bonding in THF (Figure 2a).

A blue shift in the frequencies of amide A and ester CO groups of oxalamide **3** in toluene (Figure 2b) is consistent with those observed in THF (Figure 2a). In contrast to compound **4** whose amide A region contains only associated NH groups, the amide A band of compound **3** is broadened and exhibits a shoulder at 3427 cm^{-1}, indicating the presence of nonbonded states in toluene (Figure 2b).

To determine whether the NH···OC hydrogen bonds are inter- or intramolecular, the effect of dilution on the IR behavior was tested (Figure 2c). If the ratio of associated and free NH bands does not change during the experiment, the hydrogen bonds are intramolecular. Otherwise, the disproportionate strengthening of the free NH bands indicates the presence of intermolecular aggregates.[60] At increasing dilutions of THF solutions of **3** and **4** (Figure S3 in the Supporting Information) and toluene solution of **4** (Figure 2c), no blue shifts were observed in the amide A region, indicating the absence of intermolecular aggregates. However, at an 8-fold dilution of the toluene solution, the associated NH bands of **3** were reduced by up to 30%, while the intensities of the corresponding free NH bands were reduced to a lesser extent (13%). These data demonstrated that the intramolecular associations of oxalamide **3** in toluene predominate, followed by a small population of its aggregates (Figure 2c).

The dominant red shift in the amide A region of the IR spectrum in the solid state of compound **4** indicates hydrogen bonding of a higher degree and strength[61] compared to

https://doi.org/10.1021/acs.organomet.1c00661
Organometallics 2022, 41, 920−936

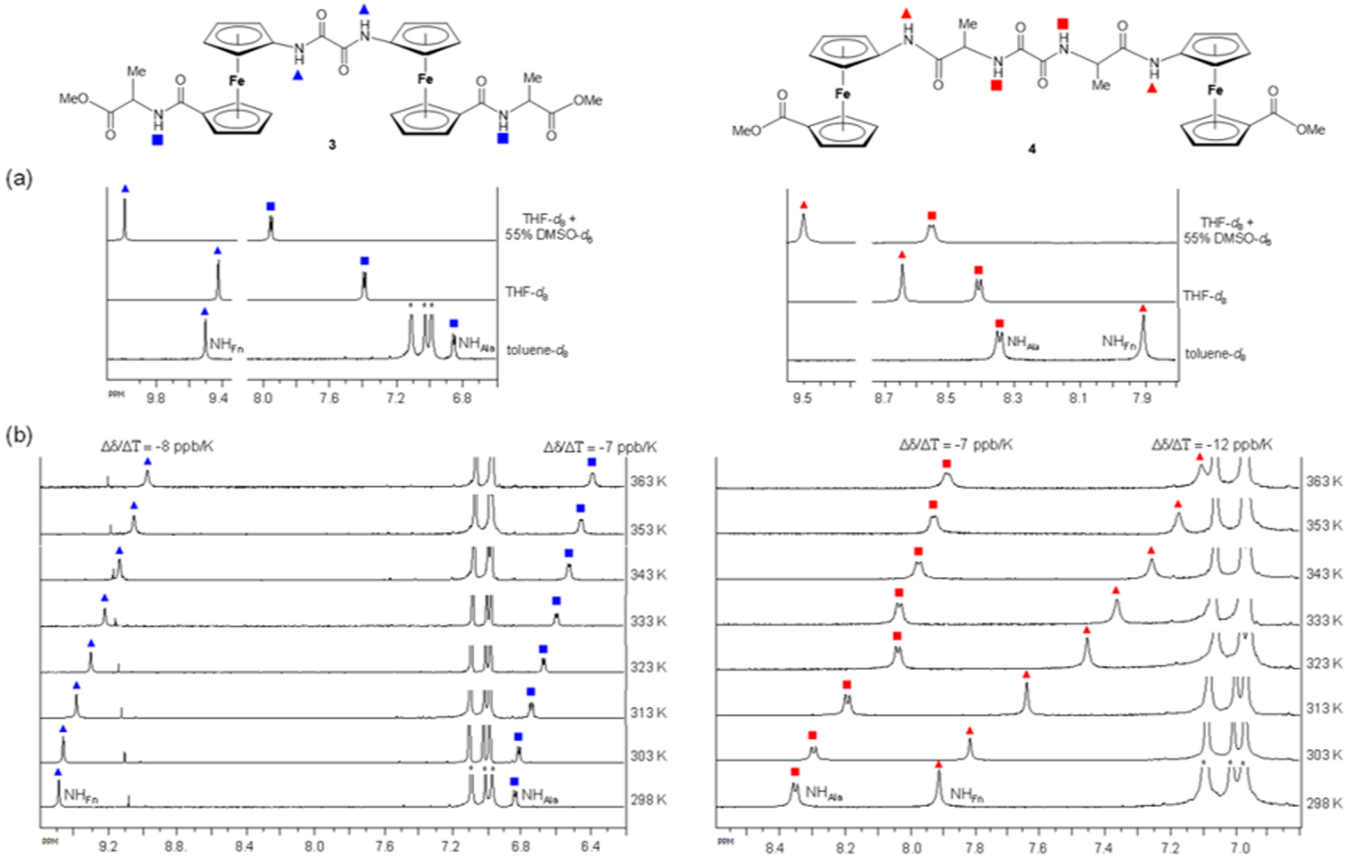

Figure 3. (a) Solvent-dependent NH chemical shifts of oxalamides **3** and **4** and (b) temperature-dependent NH chemical shifts of compounds **3** and **4** in toluene-d_8 ($c = 1 \times 10^{-3}$ M); *residual solvent.

compound **3** (Figure 2d). Moreover, the population of nonbonded groups present in the toluene solution of oxalamide **3** (shoulder at 3427 cm^{-1}, Figure 2b) is also observed in the solid state (shoulder at 3450 cm^{-1}, Figure 2d). The IR behavior of the ester CO groups of both oxalamides in the solid state (Figure 2d) is similar to that observed in the solution states (Figure 2a,b).

NMR methods based on a chemical shift not only provide information about the local magnetic environment of the nuclei but also give insight into the backbone secondary structures, the side-chain conformations, the dynamics, the solvation, and the hydrogen bonding patterns.[62] Therefore, we measured the ^1H NMR spectra in different solvents (nongelling THF, THF/dimethyl sulfoxide (DMSO) mixture, and gelling and nonbonding toluene) to assign the amide protons belonging to 1′-aminoferrocene-1-carboxylic acid (NH_{Fn}) and Ala (NH_{Ala}) but also to predict which of them is involved in hydrogen bonding. (The full NMR characterization by ^1H,$^{13}C\{^1H\}$, correlation spectroscopy (COSY), nuclear Overhauser enhancement spectroscopy (NOESY), and heteronuclear multiple bond correlation (HMBC) can be found in Figures S4−S12 and S15−S22, Supporting Information.)

Considering that the amide protons accessible to the hydrogen bond acceptor are downfield shifted,[63] the observed downfield resonances of NH_{Fn} and NH_{Ala} of compounds **3** and **4** strongly suggest that they participate in hydrogen bonding in THF and toluene, with the exception of NH_{Ala} of compound **3** whose somewhat upfield shifted resonance indicates a lower potential for hydrogen bonding in toluene (Figure 3a).

The chemical shifts of NH protons were insignificantly affected by the dilution of the THF and toluene solutions. Therefore, the intramolecular nature of the hydrogen bonds of both oxalamides in THF and toluene suggested by IR spectroscopy was further supported by concentration-independent NH chemical shifts (Figure S23, Supporting Information). The hydrogen-bonded and solvent-shielded protons are less affected by solvent exchange, while the solvent-exposed protons move upfield upon the change of the solvent from a nonbonding to proton-accepting solvent.[46,64] Therefore, we compared the chemical shifts of the NH_{Fn} and NH_{Ala} protons of the goal compounds in toluene, THF, and THF/DMSO mixture to estimate the strength of hydrogen bonds (Figure 3a). The most pronounced change in the chemical shift of the amide proton during the transition from pure toluene to the weak proton acceptor THF was observed for NH_{Fn} of compound **4** ($\Delta\delta$ = 0.8 ppm), indicating its participation in weaker intramolecular hydrogen bonding, while the slight shifts of NH_{Fn} of compound **3** and NH_{Ala} of compound **4** ($\Delta\delta$ < 0.1 ppm) indicate the preservation of IHBs in THF. A similar pattern of solvent sensitivity was registered in the mixture with 55% DMSO in THF. Therefore, the larger downfield shift of the NH_{Fn} protons of compound **4** observed upon addition of DMSO ($\Delta\delta$ = 0.9 ppm) to the THF solution further confirms their solvent-exposed nature, while the almost unperturbed and solvent-shielded NH_{Fn} protons of compound **3** ($\Delta\delta$ = 0.5 ppm) and NH_{Ala} protons of compound **4** ($\Delta\delta$ = 0.15 ppm) indicate their involvement in stronger IHBs (Figure 3a). Next, the temperature dependence of the amide chemical shifts was determined to further assess hydrogen bonding and

https://doi.org/10.1021/acs.organomet.1c00661
Organometallics 2022, 41, 920−936

the temperature-dependent loss of the secondary structure.[65] Stronger hydrogen bonds are less susceptible to deformation upon heating, so the chemical shifts of the engaged amides change only slightly with elevated temperature.[66] The most pronounced upfield shift upon successive heating of 1 mM solutions of the studied compounds in toluene and THF was observed for NH_{Fn} of compound **4** ($\Delta\delta \sim 1$ ppm), which is certainly due to the involvement in weaker IHBs, as suggested by solvent-dependent NMR data.[51] The chemical shifts of NH_{Fn} of compound **3** and NH_{Ala} of compound **4**, which were found to be less sensitive to hydrogen-bond-accepting THF and DMSO, were also less affected by heating, confirming the assumption of their involvement in stronger IHBs. The plots of chemical shifts *versus* temperature for **3** and **4** in toluene are shown in Figure 3b, and the temperature-dependent ^{1}H NMR spectra of **3** and **4** in THF ($c = 1 \times 10^{-3}$ M) are given in the Supporting Information (Figures S9, S20, and S24). The alteration in amide chemical shifts with temperature (temperature coefficients, $\Delta\delta/\Delta T$) depends on the accessibility of the NH groups to the solvent, and thus provides useful information about hydrogen bonding.[18,67] While the law temperature coefficients are inherent for both solvent-exposed and solvent-shielded amide protons, their larger values indicate the initial shielding of amide groups and subsequent exposure through the unfolding of ordered structures or dissociation of aggregates upon heating.[68] Therefore, the larger temperature dependencies of NH groups of oxalamides **3** and **4** observed in toluene (Figure 3b) and THF (Figure S24 in Supporting Information) confirm previous findings on their involvement in hydrogen bonding.

Although the temperature- and solvent-dependent NMR behaviors of the NH_{Fn} and NH_{Ala} protons suggest different hydrogen bonding properties of oxalamides **3** and **4**, both tend to adopt the conformations realized by intramolecular hydrogen bonding engagement. Considering the IR and NMR data of compound **3** consistent with the hydrogen bonding role for amide carbonyl groups (CO_{Fn}) and NH_{Fn} protons, the observed interchain NOE contacts $NH_{Fn} \rightarrow NH_{Ala}$ and $NH_{Fn} \rightarrow CH_{3Ala}$ support the presence of $NH_{Fn}\cdots OC_{Fn}$ IHBs (Figure S25 in the Supporting Information). As for oxalamide **4**, the involvement of ester carbonyl groups and NH_{Ala} protons in IHBs is suggested by IR and NMR spectral studies, and therefore the NOE contacts $CH_{3COOMe} \rightarrow NH_{Ala}$ and $CH_{3COOMe} \rightarrow CH_{3Ala}$ detected in its spectra further confirm the presence of $NH_{Ala}\cdots OC_{COOMe}$ intramolecular hydrogen bonds (Figure S25 in the Supporting Information).

Circular Dichroism (CD) Study. Circular dichroism (CD) is a widely used method to study the secondary structure, folding behavior, and binding properties of proteins.[69] Previous work on ferrocene peptides showed that introduction of a ferrocene moiety into the chiral peptide induced IHBs between the podand peptide chains[12,17,18,70] that increased the intensity of spectral bands at 480 nm. The most pronounced Cotton effects were observed in CD spectra of symmetrically disubstituted ferrocene peptides stabilized by two interstrand IHBs,[18] while the reduction of hydrogen bonding caused not only the loss of CD activity but also the decrease of the level of chiral organization. Moreover, the right-handed helical structures and the positive Cotton effect arose if the L-amino acid was proximal to the ferrocene core.

Although the goal compounds contain an L-Ala moiety, their Cotton effects are not only different in magnitude but also differ in signs (Figure 4). While the expected positive Cotton

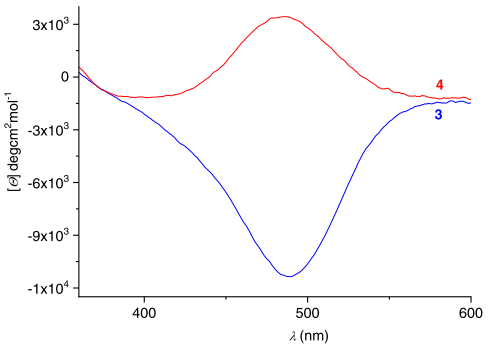

Figure 4. Cotton effects in chirality-organized ferrocene oxalamides **3** and **4** in toluene ($c = 5 \times 10^{-4}$ M).

effect in toluene was registered in the CD spectrum of compound **4**, the opposite and ~3-fold stronger CD activity was observed for compound **3**. The obtained different CD signatures showed the influence of constitutional isomerism on chiral organization. A higher degree of chiral organization in compound **3** may be attributed to the presence of stronger IHBs, as suggested by the NMR data of its amide protons, which are less sensitive to solvent and temperature effects than the hydrogen-bonded amide proton of its constitutional isomer **4**.

X-ray Diffraction. Although we used the same crystallization procedure for both oxalamides, *i.e.*, recrystallization from a solution of THF and dichloromethane, only compound **3** gave a single crystal of suitable quality for X-ray structural analysis (Table S26 in the Supporting Information). Two symmetry-independent molecules are present, labeled **A** and **B**, which have quite different conformations (Figure 5a) and are stabilized by IHBs. In both molecules, there is an $NH_{Ala}\cdots OC_{Fn}$ hydrogen bond linking two pendant groups of different ferrocenyl units (Figure 5b). There is also a pair of hydrogen bonds, $NH_{Fn}\cdots O{=}C_{COOMe}$ (oxygen from the carbonyl group) and $NH_{Fn}\cdots OCH_3$ (oxygen from the alkoxy group). However, **A** differs from **B** in its ability to form intermolecular hydrogen bonds: a free NH_{Ala} group participates in a hydrogen bond with an OC_{Fn} group on another ferrocenyl moiety. For more details on crystal packing, see the Supporting information (Figure S27).

Computational Study. The density functional theory (DFT) study provided additional analysis of the conformational preferences of oxalamides **3** and **4**. A detailed conformational study started from a set of the most stable conformers obtained by molecular mechanics calculation, which were further reoptimized by DFT in implicitly modeled solvents, THF and toluene. The QTAIM theory allowed us to calculate topological parameters at bond critical points between hydrogen bond acceptors and hydrogens and to confirm the existence of hydrogen bonds, according to Koch and Popelier's criteria. The results are summarized in Figure 6 and in Table S29 and Figures S30−S38 in the Supporting Information. Conformers are sorted by increasing relative energies starting from the most stable ones from each series (labeled **3-1** and **4-1**). As expected, all conformers show a highly organized network of hydrogen bonds involving either NH_{Ala} or NH_{Fn} amino groups directly attached to the ferrocene core. The most stable conformers of compound **3**, in which two ferrocene cores are linked by the short oxalamide spacer, contain at least one 9-membered ring connected by $NH_{Fn}\cdots OC_{Ala}$ and one 13-membered ring linked by an $NH_{Ala}\cdots OC_{Fn}$

https://doi.org/10.1021/acs.organomet.1c00661
Organometallics 2022, 41, 920−936

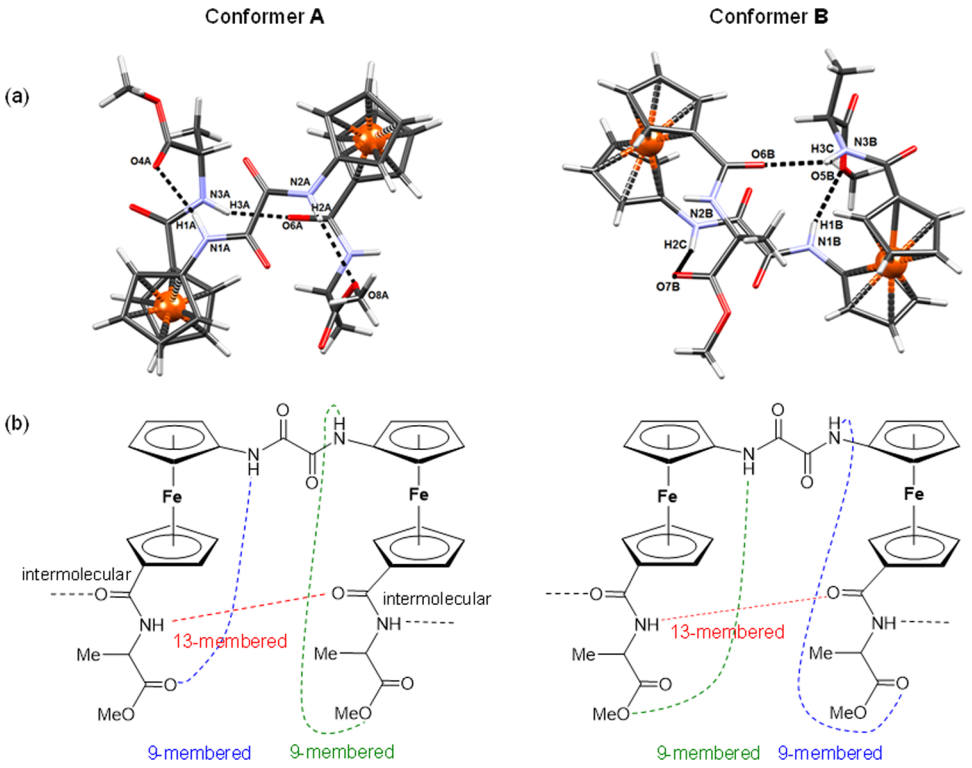

Figure 5. (a) Two conformers of **3**, labeled as **A** and **B**, with intramolecular hydrogen bonds shown as black dotted lines and (b) schematic drawing of intra- and intermolecular hydrogen bonds (dotted lines) in conformers **A** and **B**.

hydrogen bond (Figures 5, S30, and S31). All hydrogen bonds are formed between oppositely attached substituents, driving the formation of a relatively compact spherical structure, leaving only one nonbonded NH group. Due to a longer dipeptide spacer (Ala−Ala) between the bulky ferrocene units in the conformers of oxalamide **4**, this structure is more prone to rotation around single bonds across the spacer. In this way, a suitable position of all good hydrogen bond donors and acceptors is easily achieved to form hydrogen bonds in a C2 symmetrical geometry of **4**. Two pairs of equivalent hydrogen bonds are established between the oppositely attached substituents, $NH_{Fn}\cdots OC_{COOMe}$ and $NH_{Ala}\cdots OC_{COOMe}$, defining 15- and 12-membered rings, respectively.

The computationally characterized conformers agree well with the experimental findings and confirm the involvement of all NH groups of **4** in intramolecular hydrogen bonding compared to some free NH groups of **3** for which there is a higher probability of IHBs. The DFT study fits well with the results of NMR analysis in different solvents, suggesting a lower involvement of NH_{Ala} in hydrogen bonding as it remains unbound in the most stable conformers of compound **3**. Interestingly, the second most stable conformer (**3-2**) and conformer **B** from the X-ray-determined structure, with the only remaining accessible NH_{Ala} group not involved in hydrogen bonding, are almost identical (Figure S32 in the Supporting Information). In comparison, conformer **A** with the NH_{Ala} group involved in intermolecular hydrogen bonding is similar to **3-3** but differs mainly in the orientation of the terminal ester group (Figure S33 in the Supporting Information). In summary, neither of the two conformers obtained crystallographically is identical to the most stable conformer obtained in solution (**3-1**), suggesting additional stabilization by intermolecular interactions that overcome the energy penalty involved in the conformational transition from **3-1** to **3-2** and/or **3-3**, as previously observed for similar compounds.[71]

In addition, we calculated electronic circular dichroism (ECD) spectra (Figure S34 in the Supporting Information) for the most stable conformers of oxalamides **3** and **4**. While there is a fairly good matching between the time-dependent DFT (TD-DFT) calculated and experimental CD spectra in the region of the ferrocene chromophore near 480 nm for compound **3**, due to the same sign of the Cotton effect for all of the energetically favorable conformers, there are some discrepancies for compound **4**. Although the energetically most favorable **4-1** near 480 nm shows the opposite sign of the Cotton effect, the second one (**4-2**) follows the sign in the experimentally determined CD spectra. Taking into account that the use of different DFT methods may affect the relative distribution of conformers and/or even alter the energy levels, special care should be taken when interpreting these results and selecting the appropriate method and cutoff energy level for a selection of the abundant conformers. Nevertheless, among the two most stable conformers of **4**, there is obviously one that exhibits a very similar ECD spectrum to the experimentally determined ones.

The main character of the CD transition in the region around 480 nm was depicted by natural transition orbitals (NTO), which provide a concise representation for electronic excitations as a single excitation from an occupied to a virtual NTO orbital. In addition, density difference plots were depicted for each transition, showing regions of increased and decreased electronic density (Figures S35−S38 in the Supporting Information). The electronic transitions labeled 5−8, which occur near 480 nm, are in good agreement with the ligand field theory showing the low-lying excited states of

https://doi.org/10.1021/acs.organomet.1c00661
Organometallics 2022, 41, 920−936

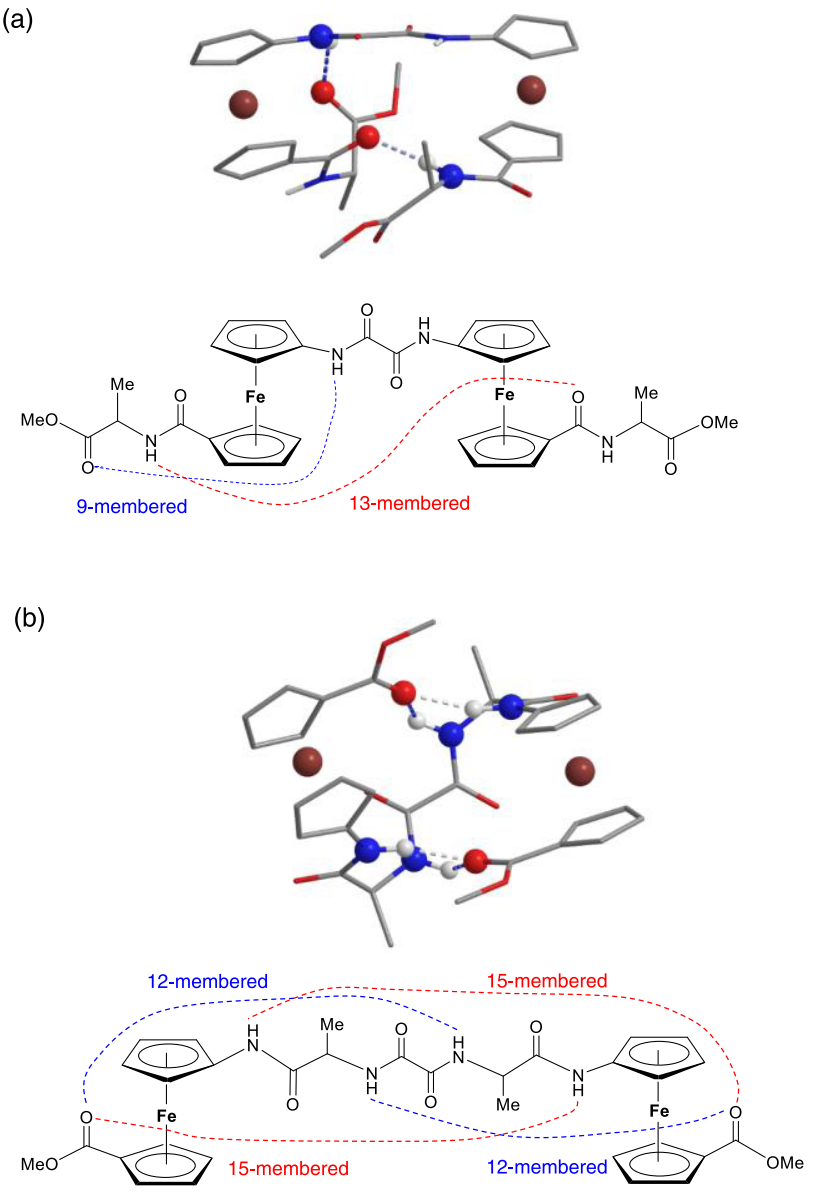

Figure 6. DFT-optimized geometries of the most stable conformers and the scheme of the identified intramolecular hydrogen bond patterns in **3** (a) and **4** (b). Hydrogens not involved in hydrogen bonds are omitted for clarity.

ferrocene corresponding to the d−d transitions on iron.[72] Since two substituents locked by intramolecular hydrogen bonds achieve a well-organized right- or left-handed helicity according to orbital diagrams, local excitation depends on the relative orientation (left or right) of the IHB-involved oxalamide and/or amide groups directly attached on both cyclopentadienyl rings and certainly plays a crucial role in defining the sign in the CD spectrum.

Gelation and Morphological Studies. The transmission electron microscopy (TEM) study of a toluene solution of oxalamide **3** revealed the formation of self-assembled nanostructures, namely isolated nanospheroids or vesicle-like morphology with irregular size (Figure 7d,e). Interestingly, sonication of a freshly prepared solution of **3** for 2 min results in a viscous gel-like material [not a true gel, (Figure 8a−c)], which converts into a heterogeneous solution containing broken gel-like aggregates under mechanical stimuli. Moreover, the viscous gel-like material collapses into a partially precipitated heterogeneous solution over time. It is worth mentioning that the system is thermoreversible between the clear solution and the viscous gel-like material. The sonication-induced freshly prepared viscous gel-like material was examined by TEM, which shows the formation of interlinked or fused vesicles with a diameter of 450 nm (Figure 8d). The formation of the fused nanovesicles occurs under sonication only and is believed to be responsible for the increase in viscosity and loose gel-like self-assembled soft materials.

Similarly, the self-assembly of compound **4** in toluene was studied. Cooling of the hot monomeric solution of **4** results in a heterogeneous mixture solution containing solid aggregates (no solid-like gel-phase material, Figure 7a−c). TEM studies show the formation of long nanofibers. However, these self-assembled nanofibers are neither dense enough nor cross-linked, which explains the reason for the inability of the system to form a stable gel or stable viscous materials (Figure 7f,g). However, if the hot solution of **4** is cooled to room temperature and then immediately sonicated (for 1 min), a solid-like self-standing gel-phase material is formed (Figure

https://doi.org/10.1021/acs.organomet.1c00661
Organometallics 2022, 41, 920−936

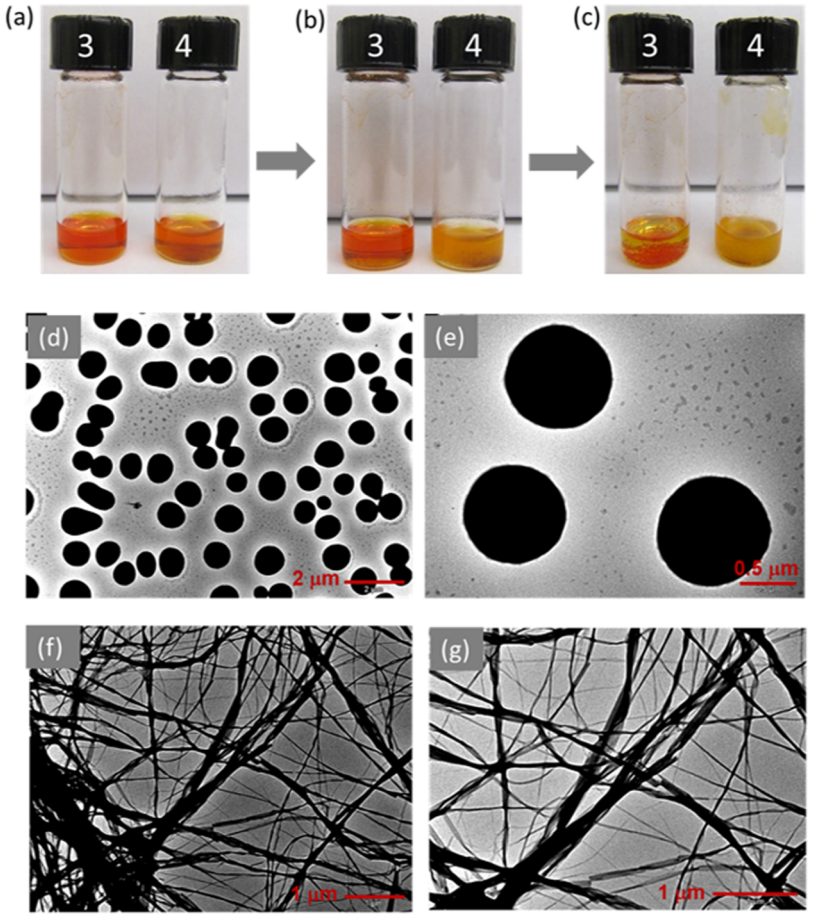

Figure 7. Preparation of the self-assembled viscous material of oxalamides **3** (left) and **4** (right) in toluene without application of sonication. (a) Photographs of two oxalamides in toluene at elevated temperature. (a) Transforms to (b) upon cooling to room temperature. (b) Transforms to (c) upon standing over a period of time (1 h). (d–g) TEM images of self-assembled **3** (d, e) and **4** (f, g) with increasing magnification from left to right. The TEM samples were taken after heating and subsequent cooling ((b) vials).

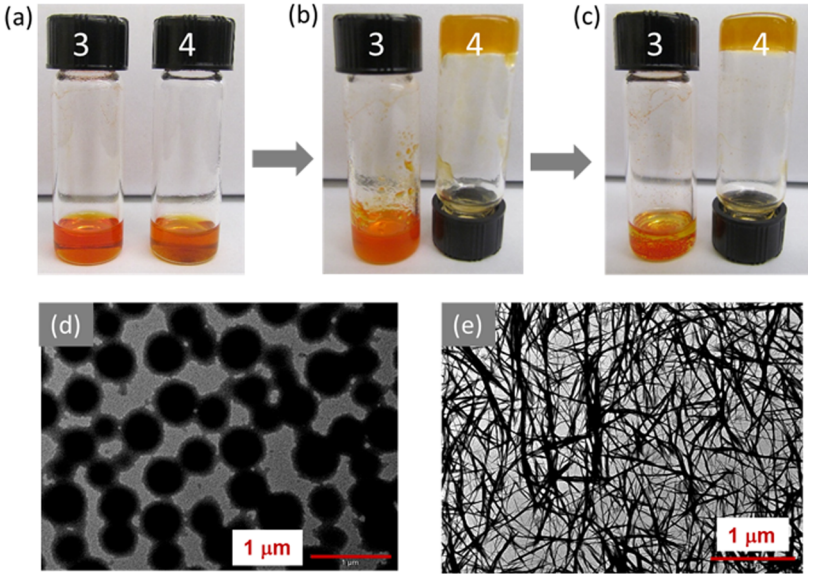

Figure 8. Preparation of self-assembly of oxalamide **3** (left vial) and oxalamide **4** (right vial) in toluene upon sonication. (a) Photograph of hot solutions for two oxalamides showing these are complete solutions, (a) transforms to (b) upon cooling to room temperature with the application of sonication (the image (b) shows the formation of a viscous gel-like material and a solid-like gel-phase material for of oxalamide **3** and oxalamide **4**, respectively), and (b) transforms to (c) upon standing for an hour, showing the complete collapse of the loose gel-like material in the case of oxalamide **3**, whereas oxalamide **4** gel remains stable. (d, e) TEM images of sonication-induced self-assembled **3** (d) and **4** (e). The samples for the TEM experiment were taken from (b) vials.

https://doi.org/10.1021/acs.organomet.1c00661
Organometallics 2022, 41, 920–936

Table 1. IC_{50} Values for Oxalamides 3, 4, III, and Cisplatin Calculated for HeLa, MCF7, HepG2, and HEK293T Cells

	IC_{50} (μM)			
	HEK293T	MCF-7	HepG2	HeLa
3	66.84 ± 7.38	47.78 ± 2.58	71.38 ± 5,63	45.26 ± 4.27
4	97.65 ± 9.21	101.68 ± 4.94	135.36 ± 6.64	105.37 ± 3.49
III[a]	N.D.	N.T.	N.D.	252.79
cisplatin		97.86[b]	15.9[c]	46.14[b]

[a]Adapted from ref 39: N.D.= not detected and N.T.= not tested in ref 39. [b]Adapted from ref 81. [c]Adapted from ref 78.

8a−c). It is noted that the time of sonication required for gel formation is shorter for compound **4** than for **3**, indicating that **4** is more susceptible to assembly by sonication. The minimum gelation concentration (mgc) for the gel of **4** was measured to be 1.42% w/v. The resulting self-standing gel is stable over a period of time. It is noted that the gel is completely thermoreversible in nature and the sol−gel transition temperature is 80 °C at mgc. Moreover, the sol−gel transition temperature increases with increasing concentration of gelator **4** (Figure S39 in the Supporting Information). Investigation of gel by TEM shows exclusively the formation of a self-assembled nanofibrillar network-like morphology (Figure 8e), which is responsible for entrapping many solvent molecules, resulting in a gel. Each fiber is a few micrometers long and the width of these fibers is in the range of 30−50 nm. More importantly, these nanofibers are relatively monodisperse in nature than the fibers (irregular nanofibers of larger size) formed without sonication, so sonication assisted the formation of a relatively monodisperse nanofibrillar network responsible for gelation.

***In Vitro* Activity of Oxalamides against Human Cell Lines.** Many oxalamide derivatives exhibit different biological activities; they can act as plant growth regulators,[73] HIV-1 protease inhibitors,[53,74] antimycobacterial agents,[75] and antitumor agents.[76,77] Therefore, the cytotoxicity of ferrocene oxalamides **3** and **4** against three tumor cell lines [MCF7 (mammary adenocarcinoma cells), HeLa (cervical adenocarcinoma cells), and HepG2 (hepatocellular carcinoma cells)] and one normal human cell line [HEK293T (embryonic kidney cells)] was investigated. Human tumor cell lines are often used to evaluate compounds of interest as potential anticancer drugs. These are then tested over a range of concentrations to determine cell growth inhibition or cytotoxicity against each cell line. These preliminary *in vitro* results are used as a screen to decide which compound or structure has the potential to be further developed as an anticancer agent. Our findings on oxalamide **III**, which showed dual biological activity on cell growth,[39] led us to believe that oxalamide-bridged ferrocenes have the potential for drug development, and we, therefore, proceeded to investigate the biological activities of such structures. HeLa, MCF7, HepG2, and HEK293T cells were treated with different concentrations of oxalamides **3** and **4** (1−200 μM) for 72 h, and then cell viability was determined by cell proliferation assay (Table 1 and Figure S40 in the Supporting Information).

The hormetic effect observed for oxalamide **III**,[39] characterized by stimulation at a low dose and inhibition at a high dose, is also evident here. A stimulatory effect on the growth of HEK293T, MCF7, and HepG2 cells (from +12 to +26%) is observed when cells are treated with 10 μM oxalamides **3** and **4**, while higher concentrations tested had an inhibitory or toxic effect.

Compared to oxalamide **III**,[39] novel oxalamides **3** and **4** contain additional hydrogen bonding sites that allow the formation of additional IHBs. IHBs are essential in biochemistry and chemistry. They affect the electronic distribution, molecular geometry, shape, and conformation of bioactive molecules and thus significantly impact molecular properties, function, and interaction.[79] Compared to the IC_{50} value for the oxalamide **III** obtained in our work,[39] the novel oxalamides **3** and **4** possess a stronger antiproliferative effect on human cell lines. The oxalamide **III** produced the highest cytotoxic effect against HeLa cells with an IC_{50} value of 252.79 μM, while no IC_{50} values were calculated for HEK293T and HepG2 cells, as no 50% inhibition was observed in the applied concentration range. Oxalamides **3** and **4** have lower IC_{50} values (Table 1) than oxalamide **III**, implying that they are more potent as potential anticancer compounds, *i.e.*, the increase in intramolecular hydrogen bonding in **3** and **4** is shown to modulate not only the chemical but also the biological properties of the new compounds. When comparing oxalamides **3** and **4**, **3** was not only involved in stronger IHBs but also has a stronger inhibitory effect on all cell lines, with HeLa cells being the most sensitive to the oxalamide-bridged ferrocenes prepared in our group. This result may indicate specificity to cell type and/or tumors. The IC_{50} values obtained for oxalamides **3** and **4** are higher than those obtained for cisplatin, the reference drug frequently used in antitumor assays, which has IC_{50} values ranging from 0.1 to 15 μM, depending on the cell line.[50,70e,80] Also, there is a report on the IC_{50} value for cisplatin based on 768 cell lines screened and determined as a geometric mean to be 26.4 μM.[81]

Nevertheless, we believe that it is worthwhile to continue studies on the anticancer activity of ferrocene oxalamides since the new oxalamide **3**, which is equipped with additional hydrogen bonding sites, has more than 5-fold improved anticancer activity compared to the previous oxalamide **III**. In most studies involving different oxalamide complexes, they had weaker antitumor activity than cisplatin, but this did not discourage researchers to proceed with further systematic structure-based design, synthesis, functional, and biological evaluation of oxalamide derivatives. A good example is dicopper(II) complexes bridged with asymmetric *N*,*N*′-bis-(substituted)oxalamide and containing various terminal ligands. It has been shown that the DNA-binding and cytotoxic activities can be tuned by varying the substituent groups of the bridging ligands, which is very useful for the design of new oxalamide drugs.[48,50]

During the *in vitro* antiproliferative assay, it is common to examine the cells daily with an inverted light microscope to see if there are any visible changes in the treated cells. Changes in the morphology of ferrocene oxalamide-treated cells compared to control cells were observed after approximately 48 h of treatment. The decreased density of monolayers, loss of contact between adjacent cells, and rounding of treated cells

https://doi.org/10.1021/acs.organomet.1c00661
Organometallics 2022, 41, 920−936

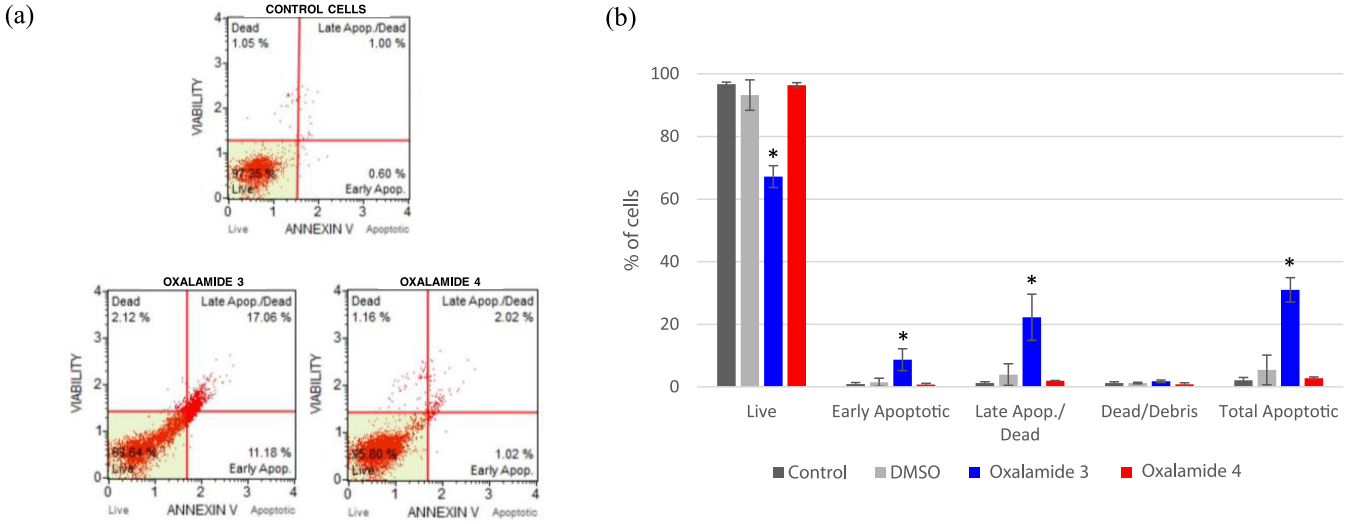

Figure 9. (a) Representative histograms of control and oxalamide-treated (100 μM) HeLa cells obtained by the MuseTM Annexin V & Dead Cell Assay after 72 h of treatment, (b) distribution of cell populations for control, DMSO, oxalamide **3**, and oxalamide **4**-treated HeLa cells. Results are expressed as % of control cells ± standard deviation (S.D.) (n = 2). Means with an asterisk indicate significant differences ($p < 0.05$) *versus* control/ untreated cells.

were noted. Therefore, to further investigate the possible type of cell death associated with the observed cytotoxicity of oxalamides **3** and **4**, flow cytometric analysis of HeLa cells was performed using Muse Annexin V & Dead Cell Assay. The method is based on double staining with Annexin V-PE and 7-aminoactinomycin D (7-AAD), which allows four different cell populations to be discriminated and quantified, as shown in Figure 9.

The results shown in Figure 9 are consistent with the evaluation of anticancer activity assessed by the antiproliferation assay, in which oxalamide **3** gave a higher percentage of inhibition than oxalamide **4**. A significant difference between control HeLa cells and oxalamide-treated cells was observed in the case of **3** in all cell populations. Analysis of HeLa cells treated with **3** (100 μM ~ 2 × IC_{50} value) revealed a percentage of live cells of 67.17 ± 3.49%, while the overall percentage of apoptotic cells was 30.995 ± 3.90%, with late apoptotic/dead cells dominating (up to 22.28%).

Accordingly, cell death by apoptosis might be related to the observed cytotoxicity of oxalamide **3** against cancer cell lines. When it comes to oxalamide-bridged ferrocenes, this is the first report on the analysis of cell death induced by these compounds, but further work is needed to gain a better insight into the mechanism of action and the specific pathways involved in the observed cytotoxicity. It is well known that dysregulation of apoptosis can lead to uncontrolled cell survival and excessive accumulation, which, among other things, can lead to cancer development.[82] Therefore, most pharmaceutical research programs related to cancer therapies are antiapoptotic drug discovery programs that involve the exploration of metal complexes that bind to DNA,[48] the development of inhibitors for various caspases,[83] *etc.* For example, a viability screen of over 200,000 small molecules enabled the identification of oxalamides and benzothiazoles that are selectively toxic to 4 of 12 human lung cancer cell lines,[84] but although their toxicity mechanism of action is suggested, further research is needed and strongly encouraged.

CONCLUSIONS

Ferrocene peptides **1** and **2** were dimerized *via* an oxalamide link to give constitutional isomers **3** and **4**, respectively. The goal compounds **3** and **4** were subjected to spectroscopic, gelation, and cytotoxic studies to determine their conformational properties, gelation ability, and growth-inhibitory potential for cancer and normal cells.

The different conformational patterns of **3** and **4** were expected due to the different placement of hydrogen-bond-donating and -accepting sites. In addition, oxalamide **4** contains a longer Ala−Ala spacer, and rotation around the numerous single bonds between two ferrocene units was also expected to contribute to its increased flexibility. IR data in toluene indicate that exclusively, the NH groups of **4** are involved in intramolecular hydrogen bonds (IHBs). In comparison, the NH groups of **3** are mainly involved in IHBs, but the presence of free states and aggregates has also been suggested. Moreover, based on the IR and NOE data, the carbonyl groups of oxalamide units are not involved in IHBs. Compared to oxalamide **4**, **3** showed a ~3-fold stronger Cotton effect, indicating a higher degree of chiral organization. The spectroscopic data were confirmed by DFT calculations. Crystallographic analysis of oxalamide **3** revealed the existence of two symmetry-independent molecules with different conformations but with the common feature of noninvolvement of oxalamide carbonyl groups in IHBs.

Due to their limited solubility, toluene was chosen as a suitable solvent for the gelation study of oxalamides **3** and **4**. These compounds were not able to gelate toluene without sonication. However, sonication-assisted gelation resulted in a viscous gel-like material for **3**, which collapsed on standing, and a solid-like gel-phase material for **4**, which was found to be stable. Considering that the oxalamide **III** and its alanine analogue **3**, which contain an −NH−CO−CO−NH− unit between the ferrocene moieties were unable to gelate the tested solvents, future work on ferrocene−oxalamide gelators will be directed toward more flexible analogues of gelator **4** with longer spacers between the ferrocene units and the oxalamide bridge.

https://doi.org/10.1021/acs.organomet.1c00661
Organometallics 2022, 41, 920−936

A hallmark of targeted cancer therapies is selective toxicity among cancer cell lines. Therefore, in this *in vitro* study, we demonstrated that oxalamide-bridged ferrocenes exhibited growth-inhibitory properties on a cultured human tumor cell line, likely related to cell death by apoptosis. Although the growth inhibition is less pronounced than that of cisplatin, it is worth noting that the cytotoxicity of oxalamide **3** is weaker for the normal HEK293T cells than for the HeLa and MCF7 cancer cell lines, leading us to believe that oxalamide **3** has the potential for drug development as an anticancer agent. However, this potential needs to be confirmed by additional characterization of compound **3** in various pharmacological studies as well as *in vivo* toxicity evaluation. It should also be noted that the above-mentioned results on the structure–activity relationship of oxalamide-bridged ferrocenes are an initial study, which can serve for further investigations on this and similar ferrocene derivatives bridged with oxalamide moiety. Further cellular experiments are required to fully understand the mechanism of anticancer activity of these systems and to verify the correlation between the observed anticancer activity and the effects of the substituent groups, which could then serve as a good basis for the rational design of new therapeutic agents.

EXPERIMENTAL SECTION

Materials and Methods. All reactions were carried out under an argon atmosphere. CH_2Cl_2 used for the synthesis was dried (P_2O_5), distilled over CaH_2, and stored over molecular sieves (4 Å). Oxalyl chloride 98% (Acros Organics) was used as received. Ferrocene precursors Boc–NH–Fn–CO–Ala–OMe (**1**)[13,14] and Boc–Ala–NH–Fn–COOMe (**2**)[15] (Fn = ferrocenylene) were prepared by multistep reactions starting from 1′-aminoferrocene-1-carboxylic acid,[85] following our previously described procedures. Their spectral data are in complete agreement with literature data. The products were purified by preparative thin-layer chromatography on silica gel (Merck, Kieselgel 60 HF_{254}) using a CH_2Cl_2/EtOAc mixture as an eluent. The clean NMR spectra and high-performance liquid chromatography (HPLC) traces are provided in Supporting Information as proof of purity (Figures S2, S4, S8, S11 (**3**) and S14, S15, S19, and S22 (**4**)). Infrared spectra were recorded in THF and toluene solutions [for spectroscopy Uvasol, Merck] between NaCl windows using a Bomem MB 100 mid-FTIR spectrometer [(s) = strong, (m) = medium]. The ^1H and $^{13}C\{1H\}$ NMR spectra were recorded at 600 and 150 MHz, respectively, using a Bruker Avance spectrometer at Ruđer Bošković Institute, and were referenced to the residual solvent peak [THF-d_8 (^1H: 1.72 and 3.58 ppm, ^{13}C: 25.31 and 67.21 ppm), toluene-d_8 (^1H: 2.08, 6.97, 7.01 and 7.09 ppm)]. In the case of the THF-d_8/DMSO-d_6 mixture, calibration was performed using Me_4Si as an internal standard (^1H: 0 ppm). Double resonance experiments (COSY, NOESY, HMBC) were performed to assist in the signal assignment [(s) = singlet, (d) = doublet, (m) = multiplet]. Unless otherwise stated, all spectra were recorded at 298 K. NMR titrations were performed by adding 10 μL portions of DMSO-d_6 to NMR tubes containing THF-d_8 solutions of the peptides under study ($c = 1 \times 10^{-3}$ M). Spectra were recorded after each addition, and DMSO-d_6 was added until no change in the chemical shift of the amide protons was observed. CD spectra were recorded using a Jasco-810 spectropolarimeter in toluene. Mass spectra were measured using a liquid chromatography-mass spectrometry (LC-MS) system coupled to a triple-quadrupole mass spectrometer, operating in a positive electrospray ionization (ESI) mode (H_2O/MeOH = 80/20). High-resolution mass spectra were acquired using a 4800 MALDI TOF/TOF-MS analyzer. Single-crystal measurements were performed on an Oxford Diffraction Xcalibur Nova R.

Synthesis of –[CO–NH–Fn–CO–Ala–OMe]$_2$ (3). The HCl gas was bubbled through the suspension of the Boc–NH–Fn–CO–Ala–OMe (**1**)[13,14] (137 mg, 0.318 mmol) in dry CH_2Cl_2 (5 mL) at 0 °C. After 30 min, the solvent was evaporated *in vacuo*, leaving a dark orange hydrochloride salt, which was then suspended in a cold CH_2Cl_2 (8 mL) and treated with Et_3N to pH ∼ 8 to afford free unstable amine NH_2–Fn–CO–Ala–OMe. The mixture of oxalyl chloride (0.027 mL, 0.318 mmol) and pyridine (0.1 mL) in CH_2Cl_2 (2 mL) was vigorously stirred and cooled (ice) and the free amine was added dropwise. Then, the reaction mixture was heated and stirred at room temperature for next 2 h until TLC monitoring showed complete conversion of the starting material. Washing with a 10% solution of citric acid, a 5% solution of $NaHCO_3$ and brine, drying over Na_2SO_4, and evaporation *in vacuo* gave the crude product, which was purified by TLC (CH_2Cl_2/EtOAc = 1:1.5) to give compound **3** as a yellow solid (R_f = 0.48; 79.3 mg, 70%). mp 96–98 °C. IR (THF) $\tilde{\nu}_{max}/cm^{-1}$: 3569, 3504 vw ($NH_{free}$), 3338 m ($NH_{assoc.}$), 1742 s, 1683 s, 1659 s, 1638 m (C═O), 1535 m (amide II). IR (toluene) $\tilde{\nu}_{max}/cm^{-1}$: 3427 vw ($NH_{free}$), 3378 m ($NH_{assoc.}$), 1738 m, 1680 s, 1652 s (C═O), 1533 m (amide II). ^1H NMR (THF-d_8): δ/ppm: 9.46 (s, 2H, NH_{Fn}), 7.42 (d, J = 8.6 Hz, 2H, NH_{Ala}), 5.06 (s, 2H, Fn), 4.94–4.92 (m, 4H, Fn), 4.85 (s, 2H, Fn), 4.76–4.73 (m, 2H, CH_{Ala}), 4.41–4.39 (m, 4H, Fn), 4.13–4.12 (m, 2H, Fn), 4.09–4.08 (m, 2H, Fn), 3.81 (s, 6H, OMe), 1.56 (d, J = 7.0 Hz, 6H, CH_{3Ala}). ^1H NMR (toluene-d_8): δ/ppm: 9.51 (s, 2H, NH_{Fn}), 6.90 (d, J = 7.5 Hz, 2H, NH_{Ala}), 5.16-5.14 (m, 2H, Fn), 4.99–4.97 (m, 4H, Fn), 4.89–4.84 (m, 4H, Fn + CH_{Ala}), 4.75–4.73 (m, 2H, Fn), 4.15–4.13 (m, 2H, Fn), 4.11–4.09 (m, 2H, Fn), 3.83–3.82 (m, 2H, Fn), 3.77–3.75 (m, 2H, Fn), 3.81 (s, 6H, OMe), 1.53 (d, J = 7.0 Hz, 6H, CH_{3Ala}). $^{13}C\{^1H\}$ NMR (THF-d_8) δ/ppm: 174.97 (COCOOMe), 168.89 (COFn), 159.05 ($CO_{oxalamide}$), 96.40 (Cq_{Fn}), 78.20 (Cq_{Fn}), 71.87, 70.72, 70.19, 66.67, 66.58, 63.54, 63.33 (C_{Fn}), 52.59 (OCH3), 49.09 (CH_{Ala}), 17.78 (CH_{3Ala}). ESI-MS: m/z = 737.1 [(M + Na)$^+$]. Matrix-assisted laser desorption ionization-high-resolution mass spectrometry (MALDI-HRMS) m/z = 714.1104 (calcd for $C_{32}H_{34}O_8N_4Fe_2$ = 714.1071).

Synthesis of –[CO–Ala–NH–Fn–COOMe]$_2$ (4). Oxalamide **4** was prepared starting from ferrocene-containing peptide **2**[15] (149 mg, 0.347 mmol) according to the procedure described above. R_f = 0.45; 97 mg, 78%, mp 120–122 °C. IR (THF) $\tilde{\nu}_{max}/cm^{-1}$: 3382 m, 3294 m, 3252 m ($NH_{assoc.}$), 1710 s, 1681 s (C═O), 1565 m (amide II). IR (toluene) $\tilde{\nu}_{max}/cm^{-1}$: 3305 m, 3268 m ($NH_{assoc.}$), 1705 s, 1680 s, 1650 s (C═O), 1545 m (amide II). ^1H NMR (THF-d_8): δ/ppm: 8.67 (s, 2H, NH_{Fn}), 8.44 (d, J = 8.5 Hz, 2H, NH_{Ala}), 4.73–4.71 (m, 6H, Fn), 4.67 (s, 2H, Fn), 4.49–4.47 (m, 2H, CH_{Ala}), 4.38 (s, 4H, Fn), 4.00–3.97 (m, 4H, Fn), 3.74 (s, 6H, OMe), 1.48 (d, J = 7.2 Hz, 6H, CH_{3Ala}). ^1H NMR (toluene-d_8): δ/ppm: 8.36 (d, J = 8.2 Hz, 2H, NH_{Ala}), 7.90 (s, 2H, NH_{Fn}), 4.90–4.88 (m, 2H, Fn), 4.85–4.83 (m, 2H, Fn), 4.77–4.75 (m, 2H, Fn), 4.56–4.49 (m, 4H, Fn + CH_{Ala}), 4.18–4.16 (m, 2H, Fn), 4.12–4.10 (m, 2H, Fn), 3.73–3.72 (m, 2H, Fn), 3.67–3.65 (m, 2H, Fn), 3.61 (s, 6H, OMe), 1.34 (d, J = 7.0 Hz, 6H, CH_{3Ala}). $^{13}C\{^1H\}$ NMR (THF-d_8) δ/ppm: 171.82 (CO-COOMe), 170.98 (CO_{Fn}), 160.83 ($CO_{oxalamide}$), 98.65 (Cq_{Fn}), 74.03, 73.58, 73.49, 72.55, 72.25, 63.51, 63.28 (C_{Fn}), 52.18 (OCH3), 50.85 (CH_{Ala}), 19.19 (CH_{3Ala}). ESI-MS: m/z = 737.1 [(M + Na)$^+$]. MALDI-HRMS m/z = 714.1084 (calcd for $C_{32}H_{34}O_8N_4Fe_2$ = 714.1071).

X-ray Diffraction. The crystals of **3** were very small and of rather poor quality. Therefore, X-ray diffraction measurement was only possible using a microfocus Cu radiation. Nevertheless, the quality of the measured data was poor, and rather a high R value and residual density were obtained due to a large asymmetric unit and more than 700 refined parameters.

Single-crystal X-ray measurement was performed on an Oxford Diffraction Xcalibur Nova R diffractometer with a microfocus Cu tube using graphite-monochromated Cu Kα radiation (λ = 1.54179 Å). The program package CrysAlis PRO[86] was used for data reduction and multiscan absorption correction. The structure was solved with SHELXS97[87] and refined with SHELXL97[88] using full-matrix least-squares refinement. Due to the poor quality of the diffraction data, severe isotropic restraints were used to refine the nonhydrogen atoms; some were refined as isotropic. Hydrogen atoms were treated as riding entities, using the AFIX command in SHELXL97. Since the

https://doi.org/10.1021/acs.organomet.1c00661
Organometallics 2022, 41, 920–936

configurations of the stereogenic centers are known, no Friedel pairs were measured.

Molecular geometry calculations were performed with PLATON,[89] and molecular graphics were made with ORTEP-3[90] and CCDC-Mercury.[91] The crystallographic and refinement data for the structures reported in this paper are listed in Table S1 (see the Supporting Information).

Computational Details. Conformational analyses of oxalamides were performed hierarchically in three stages. The first stage included a series of low-level optimizations with molecular mechanics, OPLS2005 force field, in MacroModel v10.3.[92−94] Based on the energy criteria, a group of a few hundreds of the most stable geometries were selected for further optimizations at the high level of theory and were run in Gaussian16.[95] All calculations were performed at the B3LYP/Lanl2DZ, and only the most stable conformers at the B3LYP/6-311+G(d,p) (LanL2DZ basis set on Fe) level of theory in THF were modeled as a polarizable continuum (IEF-PCM).[96] Vibrational analysis was performed to verify each structure as a minimum on the potential energy surface. All energies were reported as sums of electronic and thermal free energies after vibrational analysis and refer to standard Gibbs free energies at 298 K. The hydrogen bonds depicted in the figures were characterized by QTAIM theory and analyzed in AIMAll.[97] Topological parameters of the displayed bond critical points between hydrogen bond acceptors and hydrogen atoms were calculated and verified following the Koch and Popelier criteria.[98] TD-DFT was employed to calculate excited states at the same level of theory as used to optimize the conformers. The average CD spectra were calculated by weighting individual CD spectra of each conformer (from the group of the most stable conformers) with Boltzmann factors calculated at 298 K. Natural transition orbitals (NTO) and density difference plots were visualized in GaussView6.[99]

Gel Preparation. In the course of studying self-assembly, we tested the gelation behavior of compounds **3** and **4** in toluene. An amount of 7.14 mg of the tested peptides was placed in a glass vial with a screw cap and 0.5 mL of toluene was added. The suspensions were heated at ∼100 °C until complete solutions (c = 0.02 M). Then, the hot solutions were cooled to room temperature, resulting in a solution that slowly precipitated over time. To test the nanoscale morphology of the resulting assemblies, the freshly prepared solutions of aggregates were examined by transmission electron microscopy (TEM). Moreover, sonication-induced self-assembly of the peptides was also tested where the hot solutions (c = 0.02 M) were cooled to room temperature followed by sonication for 1−2 min and this led to the formation of a gel.

Biological Evaluation. *Evaluation of In Vitro Antitumor Activity.* The anticancer activity of oxalamide-bridged ferrocenes **3** and **4** was evaluated *in vitro* against four adherent human cell lines using the CellTiter 96 AQueous One Solution Cell Proliferation Assay (Promega). HEK293T (ATCC No. CRL-3216), HeLa (ATCC No. CCL-2), MCF7 (ATCC No. HTB-22), and HepG2 (ATCC No. HB-8065) cells were cultured in Dulbecco's modified Eagle's medium (DMEM) (Lonza, Belgium) supplemented with 5% (v/v) heat-inactivated fetal bovine serum (FBS) (Gibco Invitrogen Corporation, U.K.) and maintained in BioLite Petri dishes (Thermo Fisher Scientific) in an incubator with a humidified atmosphere and 5% CO_2 at 37 °C. Experiments were performed three times with five parallels for each concentration of compounds tested in BioLite 96-well plates (Thermo Fisher Scientific) seeded with exponentially growing cells at the indicated concentration (∼3 × 10^4 cells per well in 100 μL of medium) and incubated for 24 h. Both compounds were dissolved in DMSO and diluted to the required concentration with a culture medium when applied to the cells. The final concentrations of oxalamides **3** and **4** ranged from 1 to 200 μM so that the content of DMSO per well did not exceed 0.1%. The control cells were untreated cells. After treatment, the plates containing the cells were incubated for an additional 72 h, after which the CellTiter 96 AQueous One Solution Cell Proliferation Assay was performed according to the manufacturer's instructions with minor modifications. In brief, 10 μL of the CellTiter 96 AQueous One Solution Cell Proliferation Reagent was added to each well and the cells were incubated for an additional 3 h, after which the absorbance was measured at 490 nm using a microplate reader (Tecan, Switzerland). Cell viability was expressed as the percentage of treated cells over control cells. Experiments were performed three times with five parallels for each concentration of tested compounds and data were expressed as mean ± S.D. Corresponding IC_{50} values were calculated from the dose−response curves of each experiment using equations of best-fit trend lines and then the average of IC_{50} and S.D. were calculated.

Evaluation of Cell Death by Flow Cytometric Analysis. Quantitative analysis of live, apoptotic, and dead cells treated with ferrocene oxalamides **3** and **4** was performed with a Muse Cell Analyzer (EMD Millipore Corporation, Massachusetts) using a Muse Annexin V & Dead Cell Kit (Merck KGaA, Darmstadt, Germany) according to the manufacturer's specifications. In brief, HeLa cells were seeded in six-well culture plates at a density of 5 × 10^4 cells mL^{-1} (2 mL per well) and treated with a selected concentration (100 μM) of the tested compounds for 72 h. After treatment, both floating and adherent cells were collected, centrifuged (600 g min^{-1}), and suspended in a cell culture medium to adjust the cell concentration according to the manufacturer's protocol. Then, an aliquot of 100 μL of the cell suspension was added to 100 μL of the Muse Annexin V & Dead Cell Reagent and incubated for 20 min at room temperature in the dark. The cells were then analyzed using the Muse Cell Analyzer. There were two parallels for each concentration tested and each experiment was performed twice. The Muse Annexin V & Dead Cell Assay detects phosphatidylserine on the external membrane of apoptotic cells through Annexin V-PE binding, while 7-amino-actinomycin D (7-AAD) is used as a marker for dead cells. On this basis, this assay can detect four different cell populations: live (Annexin V negative and 7-AAD negative), early apoptotic (Annexin V positive and 7-AAD negative), late-stage apoptotic (Annexin V positive and 7-AAD positive), and dead cells, mainly nuclear debris (Annexin V negative and 7-AAD positive).

Statistical Analysis. All experiments were performed in triplicate for *in vitro* antitumor activity or in duplicate for cell death analysis. Results were presented as mean ± S.D. of the control cells. One-way analysis of variance (ANOVA), followed by Dunnett's significant difference test was used to determine a statistically significant (p < 0.05) difference from the control cells.

■ ASSOCIATED CONTENT

Supporting Information

The Supporting Information is available free of charge at https://pubs.acs.org/doi/10.1021/acs.organomet.1c00661.

HRMS and ESI-MS data; ^{1}H NMR, ^{13}C NMR spectra, ^{1}H−^{1}H NOESY, ^{1}H−^{1}H COSY, and ^{1}H−^{13}C HMBC spectra; concentration-dependent IR spectra; temperature- and solvent-dependent ^{1}H NMR spectra; concentration-dependent NH chemical shifts; the NOE contacts; crystallographic data collection and structure refinement details; DFT data; and effect of oxalamides on cell viability of HeLa, MCF7, HepG2, and HEK293T cell lines (PDF)

Accession Codes

CCDC 2120366 contains the supplementary crystallographic data for this paper. These data can be obtained free of charge via www.ccdc.cam.ac.uk/data_request/cif, or by emailing data_request@ccdc.cam.ac.uk, or by contacting The Cambridge Crystallographic Data Centre, 12 Union Road, Cambridge CB2 1EZ, UK; fax: +44 1223 336033. Supporting crystallographic data for this paper can be obtained free of charge *via* www.ccdc.cam.ac.uk/conts/retrieving.html (or from the Cambridge Crystallographic Data Centre, 12, Union Road, Cambridge CB2 1EZ, U.K.; fax: +44 1223 336033; or

https://doi.org/10.1021/acs.organomet.1c00661
Organometallics 2022, 41, 920−936

deposit@ccdc.cam.ac.uk). CCDC 2120366 contains the Supporting crystallographic data for this paper.

AUTHOR INFORMATION

Corresponding Authors

Heinz-Bernhard Kraatz − *Department of Physical and Environmental Sciences, University of Toronto Scarborough, Toronto, Ontario M1C 1A4, Canada; Department of Chemistry, University of Toronto, Toronto, Ontario M5S 3H6, Canada;* orcid.org/0000-0002-7149-0110; Email: bernie.kraatz@utoronto.ca

Lidija Barišić − *Department of Chemistry and Biochemistry, Faculty of Food Technology and Biotechnology, University of Zagreb, 10000 Zagreb, Croatia;* orcid.org/0000-0002-4310-4198; Email: lidija.barisic@pbf.hr

Authors

Veronika Kovač − *Department of Chemistry and Biochemistry, Faculty of Food Technology and Biotechnology, University of Zagreb, 10000 Zagreb, Croatia*

Ivan Kodrin − *Department of Organic Chemistry, Faculty of Science, University of Zagreb, 10000 Zagreb, Croatia;* orcid.org/0000-0001-6353-3187

Kristina Radošević − *Department of Biochemical Engineering, Faculty of Food Technology and Biotechnology, University of Zagreb, 10000 Zagreb, Croatia*

Krešimir Molčanov − *Division of Physical Chemistry, Ruđer Bošković Institute, 10000 Zagreb, Croatia*

Bimalendu Adhikari − *Department of Chemistry, National Institute of Technology, Rourkela, Sundargarh 769008 Odisha, India*

Complete contact information is available at: https://pubs.acs.org/10.1021/acs.organomet.1c00661

Notes

The authors declare no competing financial interest.

ACKNOWLEDGMENTS

This work was fully supported by the Croatian Science Foundation under the project IP-2014-09-7899.

REFERENCES

(1) Ren, C.; Zhang, J.; Chen, M.; Yang, Z. Self-assembling small molecules for the detection of important analytes. *Chem. Soc. Rev.* **2014**, *43*, 7257−7266.

(2) Du, X.; Zhou, J.; Shi, J.; Xu, B. Supramolecular Hydrogelators and Hydrogels: From Soft Matter to Molecular Biomaterials. *Chem. Rev.* **2015**, *115*, 13165−13307.

(3) Vujičić, N. i.; Glasovac, Z.; Zweep, N.; van Esch, J. H.; Vinković, M.; Popović, J.; Žinić, M. Chiral Hexa- and Nonamethylene-Bridged Bis(L-Leu-oxalamide) Gelators: The First Oxalamide Gels Containing Aggregates with a Chiral Morphology. *Chem.—Eur. J.* **2013**, *19*, 8558−8572.

(4) Yadav, S.; Sharma, A. K.; Kumar, P. Nanoscale Self-Assembly for Therapeutic Delivery. *Front. Bioeng. Biotechnol.* **2020**, *8*, No. 127.

(5) Adhikari, B.; Kraatz, H.-B. Redox-triggered changes in the self-assembly of a ferrocene−peptide conjugate. *Chem. Commun.* **2014**, *50*, 5551−5553.

(6) Busseron, E.; Ruff, Y.; Moulin, E.; Giuseppone, N. Supramolecular self-assemblies as functional nanomaterials. *Nanoscale* **2013**, *5*, 7098−7140.

(7) Xing, P.; Zhao, Y. Multifunctional nanoparticles self-assembled from small organic building blocks for biomedicine. *Adv. Mater.* **2016**, *28*, 7304−7339.

(8) Sun, Z.; Li, Z.; He, Y.; Shen, R.; Deng, L.; Yang, M.; Liang, Y.; Zhang, Y. Ferrocenoyl Phenylalanine: A New Strategy Toward Supramolecular Hydrogels with Multistimuli Responsive Properties. *J. Am. Chem. Soc.* **2013**, *135*, 13379−13386.

(9) Kimura, S.; Yokoya, M.; Yamanaka, M. Biolgical-stimuli-responsive Supramolecular Hydrogels toward Medicinal and Pharmaceutical Applications. *Chem. Lett.* **2021**, *50*, 459−466.

(10) Chu, C.-W.; Schalley, C. A. Recent Advances on Supramolecular Gels: From Stimuli-Responsive Gels to Co-Assembled and Self-Sorted Systems. *Org. Mater.* **2021**, *3*, 25−40.

(11) Municoy, S.; Álvarez Echazú, M. I.; Antezana, P. E.; Galdopórpora, J. M.; Olivetti, C.; Mebert, A. M.; Foglia, M. L.; Tuttolomondo, M. V.; Alvarez, G. S.; Hardy, J. G.; Desimone, M. F. Stimuli-Responsive Materials for Tissue Engineering and Drug Delivery. *Int. J. Mol. Sci.* **2020**, *21*, No. 4724.

(12) Moriuchi, T.; Hirao, T. Design of Ferrocene-Dipeptide Bioorganometallic Conjugates To Induce Chirality-Organized Structures. *Acc. Chem. Res.* **2010**, *43*, 1040−1051.

(13) Barišić, L.; Dropučić, M.; Rapić, V.; Pritzkow, H.; Kirin, S. I.; Metzler-Nolte, N. The first oligopeptide derivative of 1′-aminoferrocene-1-carboxylic acid shows helical chirality with antiparallel strands. *Chem. Commun.* **2004**, 2004−2005.

(14) Barišić, L.; Čakić, M.; Mahmoud, K. A.; Liu, Y.-N.; Kraatz, H.-B.; Pritzkow, H.; Kirin, S. I.; Metzler-Nolte, N.; Rapić, V. Helically Chiral Ferrocene Peptides Containing 1′-Aminoferrocene-1-Carboxylic Acid Subunits as Turn Inducers. *Chem.—Eur. J.* **2006**, *12*, 4965−4980.

(15) Barišić, L.; Kovačević, M.; Mamić, M.; Kodrin, I.; Mihalić, Z.; Rapić, V. Synthesis and Conformational Analysis of Methyl N-Alanyl-1′-aminoferrocene-1-carboxylate. *Eur. J. Inorg. Chem.* **2012**, *2012*, 1810−1822.

(16) van Staveren, D. R.; Metzler-Nolte, N. Bioorganometallic Chemistry of Ferrocene. *Chem. Rev.* **2004**, *104*, 5931−5985.

(17) Kovačević, M.; Kodrin, I.; Cetina, M.; Kmetič, I.; Murati, T.; Čakić Semenčić, M.; Roca, S.; Barišić, L. The conjugates of ferrocene-1,1′-diamine and amino acids. A novel synthetic approach and conformational analysis. *Dalton Trans.* **2015**, *44*, 16405−16420.

(18) Kovačević, M.; Kodrin, I.; Roca, S.; Molčanov, K.; Shen, Y.; Adhikari, B.; Kraatz, H.-B.; Barišić, L. Helically Chiral Peptides That Contain Ferrocene-1,1′-diamine Scaffolds as a Turn Inducer. *Chem.—Eur. J.* **2017**, *23*, 10372−10395.

(19) Nuskol, M.; Studen, B.; Meden, A.; Kodrin, I.; Čakić Semenčić, M. Tight turn in dipeptide bridged ferrocenes: Synthesis, X-ray structural, theoretical and spectroscopic studies. *Polyhedron* **2019**, *161*, 137−144.

(20) Martić, S.; Labib, M.; Shipman, P. O.; Kraatz, H.-B. Ferrocene-peptido conjugates: From synthesis to sensory applications. *Dalton Trans.* **2011**, *40*, 7264−7290.

(21) Beheshti, S.; Martić, S.; Kraatz, H.-B. Hierarchical Organization of Ferrocene−Peptides. *Chem.—Eur. J.* **2012**, *18*, 9099−9105.

(22) Yao, P.; Zhang, J.; You, S.; Qi, W.; Su, R.; He, Z. Ferrocene-modified peptides as inhibitors against insulin amyloid aggregation based on molecular simulation. *J. Mater. Chem. B* **2020**, *8*, 3076−3086.

(23) Liu, J.; He, P.; Yan, J.; Fang, X.; Peng, J.; Liu, K.; Fang, Y. An Organometallic Super-Gelator with Multiple-Stimulus Responsive Properties. *Adv. Mater.* **2008**, *20*, 2508−2511.

(24) Adhikari, B.; Singh, C.; Shah, A.; Lough, A. J.; Kraatz, H.-B. Amino Acid Chirality and Ferrocene Conformation Guided Self-Assembly and Gelation of Ferrocene−Peptide Conjugates. *Chem.—Eur. J.* **2015**, *21*, 11560−11572.

(25) Falcone, N.; Kraatz, H.-B. Ferrocene Peptide-based Supramolecular Gels: Current Trends and Applications. In *Advances in Bioorganometallic Chemistry*; Hirao, T.; Moriuchi, T., Eds.; Elsevier, 2019; Chapter 3, pp 57−74.

(26) Tomioka, K.; Sumiyoshi, T.; Narui, S.; Nagaoka, Y.; Iida, A.; Miwa, Y.; Taga, T.; Nakano, M.; Handa, T. Molecular Assembly and Gelating Behavior of Didodecanoylamides of α,ω- Alkylidenediamines. *J. Am. Chem. Soc.* **2001**, *123*, 11817−11818.

(27) Brinksma, J.; Feringa, B. L.; Kellogg, R. M.; Vreeker, R.; van Esch, J. Rheology and Thermotropic Properties of Bis-Urea-Based Organogels in Various Primary Alcohols. *Langmuir* **2000**, *16*, 9249−9255.
(28) Jung, J. H.; Ono, Y.; Sakurai, K.; Sano, M.; Shinkai, S. Novel Vesicular Aggregates of Crown-Appended Cholesterol Derivatives Which Act as Gelators of Organic Solvents and as Templates for Silica Transcription. *J. Am. Chem. Soc.* **2000**, *122*, 8648−8653.
(29) Jung, J. H.; Shinkai, S.; Shimizu, T. Spectral Characterization of Self-Assemblies of Aldopyranoside Amphiphilic Gelators: What is the Essential Structural Difference Between Simple Amphiphiles and Bolaamphiphiles? *Chem.—Eur. J.* **2002**, *8*, 2684−2690.
(30) Llusar, M.; Roux, C.; Pozzo, J. L.; Sanchez, C. Design of organically functionalised hybrid silica fibres through the use of anthracenic organogelators. *J. Mater. Chem.* **2003**, *13*, 442−444.
(31) Terech, P.; Scherer, C.; Demé, B.; Ramasseul, R. Aggregation of a Zn(II) Complex of a Long-Chain Triester of meso-Tetrakis[p-carboxy]phenyl Porphyrin in Hydrocarbons: Structure of Tetrameric Rodlike Assemblies. *Langmuir* **2003**, *19*, 10641−10647.
(32) Frkanec, L.; Žinić, M. Chiral bis(amino acid)- and bis(amino alcohol)-oxalamidegelators. Gelation properties, self-assembly motifs and chirality effects. *Chem. Commun.* **2010**, *46*, 522−537.
(33) Makarević, J.; Jokić, M.; Frkanec, L.; Čaplar, V.; Šijaković Vujičić, N.; Žinić, M. Oxalyl retro-peptide gelators. Synthesis, gelation properties and stereochemical effects. *Beilstein J. Org. Chem.* **2010**, *6*, 945−959.
(34) Portada, T.; Molčanov, K.; Šijaković Vujičić, N.; Žinić, M. Biphenyl Bis(amino alcohol) Oxalamide Gelators: Complex Gelation Involving Coupled Equilibria, Central-to-Axial Chirality Transfer, Diastereoisomer Interconversion, and Self-Sorting. *Eur. J. Org. Chem.* **2016**, *2016*, 1205−1214.
(35) Dabić, D.; Brkljačić, L.; Tandarić, T.; Žinić, M.; Vianello, R.; Frkanec, L.; Kobetić, R. The Metal Effect on Self-Assembling of Oxalamide Gelators Explored by Mass Spectrometry and DFT Calculations. *J. Am. Soc. Mass Spectrom.* **2018**, *29*, 103−113.
(36) Šantić, A.; Brinkkötter, M.; Portada, T.; Frkanec, L.; Cramer, C.; Schönhoff, M.; Moguš-Milanković, A. Correction: Supramolecular ionogels prepared with bis(amino alcohol)oxamides as gelators: ionic transport and mechanical properties. *RSC Adv.* **2020**, *10*, 20195.
(37) Nowick, J. S.; Chung, D. M.; Maitra, K.; Maitra, S.; Stigers, K. D.; Sun, Y. An Unnatural Amino Acid that Mimics a Tripeptide β-Strand and Forms β-Sheetlike Hydrogen-Bonded Dimers. *J. Am. Chem. Soc.* **2000**, *122*, 7654−7661.
(38) Cheng, P.-N.; Liu, C.; Zhao, M.; Eisenberg, D.; Nowick, J. S. Amyloid β-Sheet Mimics that Antagonize Amyloid Aggregation and Reduce Amyloid Toxicity. *Nat. Chem.* **2012**, *4*, 927−933.
(39) Kovač, V.; Radošević, K.; Bebek, A.; Makarević, J.; Štefanić, Z.; Barišić, L.; Žinić, M.; Rapić, V. The first oxalamide-bridged ferrocene: Facile synthesis, preliminary conformational analysis and biological evaluation. *Appl. Organomet. Chem.* **2017**, No. e3653.
(40) Tomasini, C.; Castellucci, N. Peptides and peptidomimetics that behave as low molecular weight gelators. *Chem. Soc. Rev.* **2013**, *42*, 156−172.
(41) Gómez-Castro, C.; Padilla-Martínez, I. I.; García-Báez, E. V.; Castrejón-Flores, J. L.; Peraza-Campos, A. L.; Martínez-Martínez, F. J. Solid State Structure and Solution Thermodynamics of Three-Centered Hydrogen Bonds (O●●●H●●●O) Using N-(2-Benzoylphenyl) Oxalyl Derivatives as Model Compounds. *Molecules* **2014**, *19*, 14446−14460.
(42) Nowick, J. S.; Tsai, J. H.; Bui, Q.-C.; Maitra, S. A Chemical Model of a Protein β-Sheet Dimer. *J. Am. Chem. Soc.* **1999**, *121*, 8409−8410.
(43) Dhanishta, P.; Siva kumar, P. S.; Mishra, S. K.; Suryaprakash, N. Intramolecular hydrogen bond directed stable conformations of benzoyl phenyl oxalamides: unambiguous evidence from extensive NMR studies and DFT-based computations. *RSC Adv.* **2018**, *8*, 11230−11240.
(44) Curtis, S. M.; Le, N.; Fowler, F. W.; Lauher, J. W. A Rational Approach to the Preparation of Polydipyridyldiacetylenes: An Exercise in Crystal Design. *Cryst. Growth Des.* **2005**, *5*, 2313−2321.
(45) Weiss, R. G. The past, present, and future of molecular gels. What is the status of the field, and where is it going? *J. Am. Chem. Soc.* **2014**, *136*, 7519−7530.
(46) Liu, Z.-L.; Li, L.-C.; Liao, D.-Z.; Jiang, Z.-H.; Yan, S.-P. Oxamido-Bridged Bimetallic Complexes Involving Nitronyl Nitroxide Radical Ligands: Crystal Structure and Magnetic Behavior. *Cryst. Growth Des.* **2005**, *5*, 783−787.
(47) Chen, J.-B.; Xu, M.; Zhang, J.-Q.; Sun, B.-B.; Hu, J.-M.; Yu, J.-Q.; Wang, X.-W.; Xia, Y.; Wang, Z. Modular Chiral Bisoxalamide−Copper-Catalyzed Asymmetric Oxo-Diels−Alder Reaction: Carbonyl Coordination for High Enantio- and Diastereocontrols. *ACS Catal* **2020**, *10*, 3556−3563.
(48) Li, X.-W.; Zheng, Y.-J.; Li, Y.-T.; Wu, Z.-Y.; Yan, C.-W. Synthesis and structure of new bicopper(II) complexes bridged by N-(2- aminopropyl)-N′-(2-oxidophenyl)oxamide: The effects of terminal ligands on structures, anticancer activities and DNA-binding properties. *Eur. J. Med. Chem.* **2011**, *46*, 3851−3857.
(49) Jiao, J.; Jiang, M.; Li, Y.-T.; Wu, Z.-Y.; Yan, C.-W. In Vitro Cytotoxic Activities, DNA-, and BSA-Binding Studies of a New Dinuclear Copper(II) Complex with N-[3-(Dimethylamino)propyl]-N′-(2-carboxylatophenyl)-Oxamide as Ligand. *J. Biochem. Mol. Toxicol.* **2014**, *28*, 47−59.
(50) Zheng, K.; Jiang, L.; Li, Y.-T.; Wu, Z.-Y.; Yan, C.-W. Synthesis and structure of new dicopper(II) complexes bridged by asymmetric N,N′-bis(substituted)oxamides: in vitro anticancer activity and molecular docking studies based on bio-macromolecular interaction. *RSC Adv.* **2015**, *5*, 51730−51744.
(51) Yerdelen, K. O.; Tosun, E. Synthesis, docking and biological evaluation of oxamide and fumaramide analogs as potential AChE and BuChE inhibitors. *Med. Chem. Res.* **2015**, *24*, 588−602.
(52) Yerdelen, K. O.; Koca, M.; Kasap, Z.; Anil, B. Preparation, anticholinesterase activity, and docking study of new 2-butenediamide and oxalamide derivatives. *J. Enzyme Inhib. Med. Chem.* **2015**, *30*, 671−678.
(53) Sunduru, N.; Sharma, M.; Srivastava, K.; Rajakumar, S.; Puri, S. K.; Saxena, J. K.; Chauhan, P. M. S. Synthesis of oxalamide and triazine derivatives as a novel class of hybrid 4-aminoquinoline with potent antiplasmodial activity. *Bioorg. Med. Chem.* **2009**, *17*, 6451−6462.
(54) Curreli, F.; Kwon, Y. D.; Zhang, H.; Scacalossi, D.; Belov, D. S.; Tikhonov, A. A.; Andreev, I. A.; Altieri, A.; Kurkin, A. V.; Kwong, P. D.; Debnath, A. K. Structure-Based Design of a Small Molecule CD4-Antagonist with Broad Spectrum Anti-HIV-1 Activity. *J. Med. Chem.* **2015**, *58*, 6909−6927.
(55) (a) Zweep, N.; Hopkinson, A.; Meetsma, A.; Browne, W. R.; Feringa, B. L.; van Esch, J. H. Balancing Hydrogen Bonding and van der Waals Interactions in Cyclohexane-Based Bisamide and Bisurea Organogelators. *Langmuir* **2009**, *25*, 8802−8809. (b) Žukauskaitė, A.; Moretto, A.; Peggion, C.; De Zotti, M.; Šačkus, A.; Formaggio, F.; De Kimpe, N.; Mangelinckx, S. Synthesis and Conformational Study of Model Peptides Containing N-Substituted 3-Aminoazetidine-3-carboxylic Acids. *Eur. J. Org. Chem.* **2014**, *2014*, 2312−2321.
(56) Jagesar, D. C.; Hartl, F.; Buma, W. J.; Brouwer, A. M. Infrared Study of Intercomponent Interactions in a Switchable Hydrogen-Bonded Rotaxane. *Chem.—Eur. J.* **2008**, *14*, 1935−1946.
(57) (a) Joseph, J.; Jemmis, E. D. Red-, Blue-, or No-Shift in Hydrogen Bonds: A Unified Explanation. *J. Am. Chem. Soc.* **2007**, *129*, 4620−4632. (b) Reckien, W.; Kirchner, B.; Peyerimhoff, S. D. Frequency Analysis of Amide-Linked Rotaxane Mimetics. *J. Phys. Chem. A* **2006**, *110*, 12963−12970.
(58) Ananthanarayanan, V. S.; Cameron, T. S. Proline-containing β-turns. *Int. J. Pept. Protein Res.* **1988**, *31*, 399−411.
(59) Makarević, J.; Jokić, M.; Raza, Z.; Čaplar, V.; Katalenić, D.; Štefanić, Z.; Kojić-Prodić, B.; Žinić, M. Chiral Bis(tyrosinol) and Bis(p-hydroxyphenylglycinol) Oxalamide Gelators. Influence of

https://doi.org/10.1021/acs.organomet.1c00661
Organometallics 2022, 41, 920−936

Aromatic Groups and Hydrogen Bonding on Gelation Properties. *Croat. Chem. Acta* **2004**, *77*, 403−414.
(60) (a) Rao, C. P.; Balaram, P.; Rao, C. N. R. Infrared spectroscopic study of C7 intramolecular hydrogen bonds in peptides. *Biopolymers* **1983**, *22*, 2091−2104. (b) Reddy, D. N.; Prabhakaran, E. N. Steric and electronic interactions controlling the cis/trans isomer equilibrium at X-Pro tertiary amide motifs in solution. *Biopolymers* **2014**, *101*, 66−77.
(61) Coats, J. Interpretation of Infrared Spectra, A Practical Approach. In *Encyclopedia of Analytical Chemistry*; Meyers, R. A., Ed.; John Wiley & Sons Ltd.: Chichester, 2000; pp 10815−10837.
(62) Nerli, S.; McShan, A. C.; Sgourakis, N. G. Chemical shift-based methods in NMR structure determination. *Prog. Nucl. Magn. Reson. Spectrosc.* **2018**, *106*−*107*, 1−25.
(63) (a) Gellman, S. H.; Dado, G. P.; Liang, G.-B.; Adams, B. R. Conformation-directing effects of a single intramolecular amide-amide hydrogen bond: variable-temperature NMR and IR studies on a homologous diamide series. *J. Am. Chem. Soc.* **1991**, *113*, 1164−1173. (b) Pardi, A.; Wagner, G.; Wuthrich, K. Protein conformation and proton nuclear-magnetic-resonance chemical shifts. *Eur. J. Biochem.* **1983**, *137*, 445−454.
(64) Rai, R.; Raghothama, S.; Balaram, P. Design of a Peptide Hairpin Containing a Central Three-Residue Loop. *J. Am. Chem. Soc.* **2006**, *128*, 2675−2681.
(65) Trainor, K.; Palumbo, J. A.; MacKenzie, D. W. S.; Meiering, E. M. Temperature dependence of NMR chemical shifts: Tracking and statistical analysis. *Protein Sci.* **2020**, *29*, 306−314.
(66) (a) Cierpicki, T.; Otlewski, J. Amide proton temperature coefficients as hydrogen bond indicators in proteins. *J. Biomol. NMR* **2001**, *21*, 249−261. (b) Cierpicki, T.; Zhukov, I.; Byrd, R. A.; Otlewski, J. Hydrogen Bonds in Human Ubiquitin Reflected in Temperature Coefficients of Amide Protons. *J. Magn. Reson.* **2002**, *157*, 178−180.
(67) (a) Llinás, M.; Klein, M. P. Solution conformation of the ferrichromes. VI. Charge relay at the peptide bond. Proton magnetic resonance study of solvation effects on the amide electron density distribution. *J. Am. Chem. Soc.* **1975**, *97*, 4731−4737. (b) Kessler, H. Conformation and Biological Activity of Cyclic Peptides. *Angew. Chem., Int. Ed.* **1982**, *21*, 512−523. (c) Iqbal, M.; Balaram, P. Aggregation of apolar peptides in organic solvents. Concentration dependence of 1H-nmr parameters for peptide NH groups in 310 helical decapeptide fragment of suzukacillin. *Biopolymers* **1982**, *21*, 1427−1433. (d) kumar, E. K. S. V.; Balaram, P. Stereochemistry of alpha-aminoisobutyric acid peptides in solution: helical conformations of protected decapeptides with repeating Aib-L-Ala and Aib-L-Val sequences. *Biopolymers* **1983**, *22*, 2133−2140. (e) Andersen, N. H.; Neidigh, J. W.; Harris, S. M.; Lee, G. M.; Liu, Z.; Tong, H. Extracting Information from the Temperature Gradients of Polypeptide NH Chemical Shifts. 1. The Importance of Conformational Averaging. *J. Am. Chem. Soc.* **1997**, *119*, 8547−8561. (f) Baxter, N. J.; Williamson, M. P. Temperature dependence of 1H chemical shifts in proteins. *J. Biomol. NMR* **1997**, *9*, 359−369. (g) Lee, H.-J.; Park, H.-M.; Lee, K.-B. The β-turn scaffold of tripeptide containing an azaphenylalanine residue. *Biophys. Chem.* **2007**, *125*, 117−126. (h) Appoh, F. E.; Sutherland, T. C.; Kraatz, H.-B. Changes in the hydrogen bonding pattern in ferrocene peptides. *J. Organomet. Chem.* **2004**, *689*, 4669−4677. (i) Lapić, J.; Pavlović, G.; Siebler, D.; Heinze, K.; Rapić, V. Structural, Spectroscopic, and Theoretical Study of Ferrocene Ureidopeptides. *Organometallics* **2008**, *27*, 726−735. (j) van Staveren, D. R.; Weyhermüller, T.; Metzler-Nolte, N. Organometallic β-turn mimetics. A structural and spectroscopic study of inter-strand hydrogen bonding in ferrocene and cobaltocenium conjugates of amino acids and dipeptides. *Dalton Trans.* **2003**, 210−220. (k) Bomar, M. G.; Song, B.; Kibler, P.; Kodukula, K.; Galande, A. K. An Enhanced β Turn in Water. *Org. Lett.* **2011**, *13*, 5878−5881.
(68) Stevens, E. S.; Sugawara, N.; Bonora, G. M.; Toniolo, C. Conformational analysis of linear peptides. 3. Temperature dependence of NH chemical shifts in chloroform. *J. Am. Chem. Soc.* **1980**, *102*, 7048−7050.
(69) Kelly, S. M.; Price, N. C. The use of circular dichroism in the investigation of protein structure and function. *Curr. Protein Pept. Sci.* **2000**, *1*, 349−384.
(70) (a) Adhikari, B.; Lough, J.; Barker, B.; Shah, A.; Xiang, C.; Kraatz, H.-B. Bis-amino Acid Derivatives of 1,1′-Ferrocenedicarboxylic Acid: Structural, Electrochemical, and Metal Ion Binding Studies. *Organometallics* **2014**, *33*, 4873−4887. (b) Adhikari, B.; Singh, C.; Shah, A.; Lough, A. J.; Kraatz, H.-B. Amino Acid Chirality and Ferrocene Conformation Guided Self-Assembly and Gelation of Ferrocene−Peptide Conjugates. *Chem.—Eur. J.* **2015**, *21*, 11560−11572. (c) Barišić, L.; Dropučić, M.; Rapić, V.; Pritzkow, H.; Kirin, S. I.; Metzler-Nolte, N. The first oligopeptide derivative of 1′-aminoferrocene-1-carboxylic acid shows helical chirality with antiparallel strands. *Chem. Commun.* **2004**, 2004−2005. (d) Semenčić, M. C.; Siebler, D.; Heinze, K.; Rapić, V. Bis- and Trisamides Derived From 1′-Aminoferrocene-1-carboxylic Acid and α-Amino Acids: Synthesis and Conformational Analysis. *Organometallics* **2009**, *28*, 2028−2037. (e) Chowdhury, S.; Mahmoud, K. A.; Schatte, G.; Kraatz, H.-B. Amino acid conjugates of 1,1′-diaminoferrocene. Synthesis and chiral organization. *Org. Biomol. Chem.* **2005**, *3*, 3018−3023. (f) Kovačević, M.; Molčanov, K.; Radošević, K.; Gaurina Srček, V.; Roca, S.; Čače, A.; Barišić, L. Conjugates of 1′-Aminoferrocene-1-carboxylic Acid and Proline: Synthesis, Conformational Analysis and Biological Evaluation. *Molecules* **2014**, *19*, 12852−12880.
(71) Čakić Semenčić, M.; Kodrin, I.; Barišić, L.; Nuskol, M.; Meden, A. Synthesis and Conformational Study of Monosubstituted Aminoferrocene-Based Peptides Bearing Homo- and Heterochiral Pro-Ala Sequences. *Eur. J. Inorg. Chem.* **2017**, *2017*, 306−317.
(72) Salzner, U. Quantitatively Correct UV−vis Spectrum of Ferrocene with TDB3LYP. *J. Chem. Theory Comput.* **2013**, *9*, 4064−4073.
(73) Wang, Y.; Zhu, S.; Liu, T.; Guo, B.; Li, F.; Bai, X. Identification of the rhizospheric microbe and metabolites that led by the continuous cropping of ramie (*Boehmeria nivea* L. Gaud). *Sci. Rep.* **2020**, *10*, No. 20408.
(74) Xiao, T.; Cai, Y.; Chen, B. HIV-1 Entry and Membrane Fusion Inhibitors. *Viruses* **2021**, *13*, No. 735.
(75) Krátký, M.; Stolaříková, J.; Vinšová, J. Novel Sulfamethoxazole Ureas and Oxalamide as Potential Antimycobacterial Agents. *Molecules* **2017**, *22*, No. 535.
(76) Omar, M. M.; Abd El-Halim, H. F.; Khalil, E. A. M. Synthesis, characterization, and biological and anticancer studies of mixed ligand complexes with Schiff base and 2,2′-bipyridine. *Appl. Organomet. Chem.* **2017**, *31*, No. e3724.
(77) Steeneck, C.; Kinzel, O.; Anderhub, S.; Hornberger, M.; Pinto, S.; Morschhaeuser, B.; Albers, M.; Sonnek, C.; Czekańska, M.; Hoffmann, T. Discovery and optimization of substituted oxalamides as novel heme-displacing IDO1 inhibitors. *Bioorg. Med. Chem. Lett.* **2021**, *33*, No. 127744.
(78) Pascal, F.; Bedouet, L.; Baylatry, M.; Namur, J.; Laurent, A. Comparative Chemosensitivity of VX2 and HCC Cell Lines to Drugs Used in TACE. *Anticancer Res.* **2015**, *35*, 6497−6503.
(79) Giordanetto, F.; Tyrchan, C.; Ulander, J. Intramolecular Hydrogen Bond Expectations in Medicinal Chemistry. *ACS Med. Chem. Lett.* **2017**, *8*, 139−142.
(80) Zhang, M.-J.; Liu, F.; Li, Y.-T.; Yan, C. W.; Wu, Z.-Y. Synthesis, structure, and biological active evaluation of a new cyclic tetranuclear copper(II) complex bridged both by oxamido and carboxylate groups. *J. Biochem. Mol. Toxicol.* **2018**, *32*, No. e22003.
(81) Genomics of Drug Sensitivity in Cancer. https://www.cancerrxgene.org/compound/Cisplatin/1005/overview/ic50 (accessed Feb 11, 2022).
(82) Nicholson, D. W. From bench to clinic with apoptosis based therapeutic agents. *Nature* **2000**, *407*, 810−816.
(83) (a) Talanian, R. V.; Brady, K. D.; Cryns, V. L. Caspases as targets for antiinflammatory and anti-apoptotic drug discovery. *J. Med. Chem.* **2000**, *43*, 3351−3371. (b) Ashwell, S. Caspases: Recent

https://doi.org/10.1021/acs.organomet.1c00661
Organometallics 2022, 41, 920−936

advances in small molecule inhibitors. *Exp. Opin. Ther. Pat.* **2001**, *11*, 1593−1603.
(84) Theodoropoulos, P. C.; Gonzales, S. S.; Winterton, S. E.; Rodriguez-Navas, C.; McKnight, J. S.; Morlock, L. K.; Hanson, J. M.; Cross, B.; Owen, A. E.; Duan, Y.; Moreno, J. R.; Lemoff, A.; Mirzaei, H.; Posner, B. A.; Williams, N. S.; Ready, J. M.; Nijhawan, D. Discovery of Tumor-Specific Irreversible Inhibitors of Stearoyl CoA Desaturase. *Nat. Chem. Biol.* **2016**, *12*, 218−225.
(85) Barišić, L.; Rapić, V.; Kovač, V. Ferrocene Compounds. XXIX. Efficient Syntheses of 1′-Aminoferrocene-1-carboxylic Acid Derivatives. *Croat. Chem. Acta* **2002**, *75*, 199−210.
(86) Rigaku, O. D. *PRO CrysAlis*, version 1.171.39.46; Rigaku Oxford Diffraction Ltd.: Yarnton, England, 2018.
(87) Sheldrick, G. M. SHELXT - integrated space-group and crystal-structure determination. *Acta Crystallogr., Sect. A: Found. Crystallogr.* **2015**, *71*, 3−8.
(88) Sheldrick, G. M. Crystal structure refinement with SHELXL. *Acta Crystallogr., Sect. C: Struct. Chem.* **2015**, *71*, 3−8.
(89) Spek, A. L. CheckCIF validation ALERTS: what they mean and how to respond. *Acta Crystallogr., Sect. E: Crystallogr. Commun.* **2020**, *76*, 1−11.
(90) Farrugia, L. J. ORTEP-3 for Windows - a version of ORTEP-III with a Graphical User Interface (GUI). *J. Appl. Cryst.* **1997**, *30*, 565.
(91) Macrae, C. F.; Sovago, I.; Cottrell, S. J.; Galek, P. T. A.; McCabe, P.; Pidcock, E.; Platings, M.; Shields, G. P.; Stevens, J. S.; Towler, M.; Wood, P. A. Mercury 4.0: from visualization to analysis, design and prediction. *J. Appl. Crystallogr.* **2020**, *53*, 226−235.
(92) *Maestro*, version 9.7; Schrödinger: New York, 2014.
(93) *MacroModel*, version 10.3; Schrödinger: New York, 2014.
(94) Mohamadi, F.; Richards, N. G. J.; Guida, W. C.; Liskamp, R.; Lipton, M.; Caufield, C.; Chang, G.; Hendrickson, T.; Still, W. C. Macromodel—an integrated software system for modeling organic and bioorganic molecules using molecular mechanics. *J. Comput. Chem.* **1990**, *11*, 440−467.
(95) Frisch, M. J.; Trucks, G. W.; Schlegel, H. B.; Scuseria, G. E.; Robb, M. A.; Cheeseman, J. R.; Scalmani, G.; Barone, V.; Petersson, G. A.; Nakatsuji, H.; Li, X.; Caricato, M.; Marenich, A. V.; Bloino, J.; Janesko, B. G.; Gomperts, R.; Mennucci, B.; Hratchian, H. P.; Ortiz, J. V.; Izmaylov, A. F.; Sonnenberg, J. L.; Williams-Young, D.; Ding, F.; Lipparini, F.; Egidi, F.; Goings, J.; Peng, B.; Petrone, A.; Henderson, T.; Ranasinghe, D.; Zakrzewski, V. G.; Gao, J.; Rega, N.; Zheng, G.; Liang, W.; Hada, M.; Ehara, M.; Toyota, K.; Fukuda, R.; Hasegawa, J.; Ishida, M.; Nakajima, T.; Honda, Y.; Kitao, O.; Nakai, H.; Vreven, T.; Throssell, K.; Montgomery, J. A., Jr.; Peralta, J. E.; Ogliaro, F.; Bearpark, M. J.; Heyd, J. J.; Brothers, E. N.; Kudin, K. N.; Staroverov, V. N.; Keith, T. A.; Kobayashi, R.; Normand, J.; Raghavachari, K.; Rendell, A. P.; Burant, J. C.; Iyengar, S. S.; Tomasi, J.; Cossi, M.; Millam, J. M.; Klene, M.; Adamo, C.; Cammi, R.; Ochterski, J. W.; Martin, R. L.; Morokuma, K.; Farkas, O.; Foresman, J. B.; Fox, D. J. *Gaussian 16*, revision C.01; Gaussian, Inc.: Wallingford, CT, 2016.
(96) Tomasi, J.; Mennucci, B.; Cammi, R. Quantum Mechanical Continuum Solvation Models. *Chem. Rev.* **2005**, *105*, 2999−3094.
(97) Keith, T. A. *AIMAll*, version 17.11.14; TK Gristmill Software: Overland Park, KS, 2017.
(98) (a) Koch, U.; Popelier, P. L. A. J. Characterization of C-H-O Hydrogen Bonds on the Basis of the Charge Density. *J. Phys. Chem. A* **1995**, *99*, 9747−9754. (b) Popelier, P. L. A. J. Characterization of a dihydrogen bond on the basis of the electron density. *J. Phys. Chem. A* **1998**, *102*, 1873−1878.
(99) Dennington, R.; Keith, T. A.; Millam, J. M. *GaussView*, version 6.1; Semichem Inc.: Shawnee Mission, KS, 2016.

https://doi.org/10.1021/acs.organomet.1c00661
Organometallics 2022, 41, 920−936